PREPARATION OF BIAXIALLY ALIGNED CUBIC ZIRCONIA AND CERIA FILMS ON GLASS SUBSTRATES USING ION-BEAM ASSISTED DEPOSITION

by

Angela Sue Longo

B.E.E., Electrical Engineering
University of Dayton, 1989

Submitted to the Department of
Materials Science and Engineering in Partial Fulfillment of
the Requirements for the Degree of

MASTER OF SCIENCE
in Electronic Materials
at the

Massachusetts Institute of Technology

February 1994

© Massachusetts Institute of Technology 1994
All rights reserved

Signature of Author____
Department of Materials Science and Engineering
January 14, 1994

Certified by____
Professor Michael J. Cima
Thesis Supervisor

Accepted by____
Professor Carl V. Thompson II
Professor of Electronic Materials
Chair, Departmental Committee on Graduate Studies

MAR 02 1994

ARCHIVES

PREPARATION OF BIAXIALLY ALIGNED CUBIC ZIRCONIA AND CERIA FILMS ON GLASS SUBSTRATES USING ION-BEAM ASSISTED DEPOSITION

by

Angela Sue Longo

Submitted to the Department of Materials Science and Engineering on January 14, 1994 in partial fulfillment of the requirements for the Degree of Master of Science in Electronic Materials

ABSTRACT

Yttria stabilized zirconia films and ceria films were deposited using ion assisted, electron beam deposition (IAD) on pyrex and soda lime glass substrates that were heated to 600 °C and 400 °C respectively. Films deposited under these conditions without IAD exhibit fiber texture such that preferred (100) orientation exists perpendicular to the substrate. The orientation of the films has been studied as a function of ion bombardment angle, deposition rate, ion current density, and ion beam energy. Films deposited with IAD at bombardment angles of less than 63° display strong (100) preferred orientation perpendicular to the substrate. Films having ion to atom ratios of 0.05, exhibit (220) biaxial alignment in the plane of the film. Best results were achieved for films with deposition rates of 2.4 Å/s, beam energies of 75 eV and ion fluences of 18 $\mu A/cm^2$. Increasing the beam energy to 300 eV increases the concentration of wire texture in these films. Films deposited at higher ion/atom ratios (0.11 and 0.25) produce films with alignments highly dependent on the angle of ion bombardment. Processing conditions have been shown, therefore, to effect absolute orientation, and not just the quality of the pre-existing orientation. The microstructures of the biaxially aligned films have been studied and this has allowed for a clarification of the growth mechanism of these films. A growth instability of the differing orientations during ion bombardment is shown to cause in-plane alignment rather than preferential etching of misoriented nuclei.

Thesis Supervisor: Michael J. Cima
Title: Norton Associate Professor of Ceramics

TABLE OF CONTENTS

		Page
	Title Page	1
	Abstract	2
	Table of Contents	3
	List of Figures	5
	Acknowledgments	7
Chapter 1	**Introduction**	8
	1.1 Purpose	8
	1.2 Microstructural Models for Evaporated Films	10
	1.3 Nucleation Model for Low Energy Ion Bombardment	12
Chapter 2	**Review of Related Work**	16
	2.1 Ion-beam Assisted Deposition of Zirconia Films	16
	2.2 Ion-beam Assisted Deposition of Ceria Films	18
	2.3 Growth Model for IAD of Ceria and Zirconia Films	22
	2.4 Off-normal Incidence IAD of Metal Films	25
	2.5 IAD of YSZ Films on Polycrystalline Substrates	29
Chapter 3	**Experimental Procedures**	33
	3.1 Experimental Apparatus	33
	3.2 Substrate Mounting	36
	3.3 Materials	38
	3.4 Experimental Parameters	41
	3.5 Characterization Techniques	42
Chapter 4	**Observations**	43
	4.1 YSZ Control Experiments	43
	4.2 (200) Dependence on Ion Bombardment Angle	43
	4.3 Dependence of Texture on IAD Parameters	47
	4.4 Microstructural Characterization	52
	4.5 Ion Induced Sputtering	55
	4.6 Characteristics of Ceria Films	57

Chapter 5 **Discussion** 69

5.1 Growth Model for Biaxial Alignment from IAD 69
5.2 Comparison with Related Work 72

Chapter 6 **Conclusions** 74

Chapter 7 **Future Work** 76

References 78

LIST OF FIGURES

Figure		Page
1	The three dimensional zone structure model by Thorton [18].	11
2	Growth-death competition in conical column evolution [21].	11
3	TEM micrographs showing island size and density for In deposited on Si_3N_4 [30].	15
4	XRD patterns of zirconia film grown on 300 °C (hot) and ~20 °C (cold) glass substrates with IAD using either argon or oxygen source gases [32].	17
5	XRD patterns of zirconia films grown without IAD at different substrate temperatures [35].	19
6	XRD patterns of zirconia films grown with IAD at different substrate temperatures [35].	19
7	XRD patterns of zirconia films grown with IAD at different ion beam energies [35].	21
8	Integrated counts for (111) and (220) XRD peaks in ceria films grown using IAD [37].	21
9	Film density distribution (a) without IAD, given an abrupt decrease in density at the surface; (b) after a period of ion bombardment; (c) condensing vapor refills the depleted surface region without IAD [39].	23
10	Density as a function of the ion-to-atom arrival rate for zirconia films grown using IAD [32].	24
11	Experimental and theoretical density as a function of the ion-to-atom arrival rate for ceria films grown using IAD [38].	24
12	(110) pole figure of Nb film grown without IAD [44].	26
13	(110) pole figure of Nb film grown with IAD [44].	26
14	Degree of orientation of Nb films as a function of the ion-to-atom arrival rate during deposition [44].	28
15	XRD patterns of YSZ films grown on Hastelloy using IAD [12].	30
16	(111) pole figure of YSZ film grown on Hastelloy using IAD [13].	30
17	XRD patterns of YSZ films grown on Haynes Alloy (a) with and; (b) without IAD [14].	32
18	(111) ϕ-scan of YSZ grown on Haynes Alloy with IAD [14].	32
19	Schematic of ion-beam assisted deposition system.	34
20	Schematic of Ion Tech 3RF-1200-100 ion source.	35
21	Silver paste curing schedule.	37
22	Crystal structures of YSZ, BYC, and {001} plan views of each structure [1].	39
23	Binary phase diagram of ZrO_2 and $YO_{1.5}$ [50].	40
24	X-ray diffraction patterns of YSZ films on Pyrex deposited at (a) 200 °C and; (b) 600 °C.	44
25	(111) pole figure of YSZ film on Pyrex deposited without IAD.	45

Figure **Page**

26 XRD peak intensity versus ion bombardment angle for YSZ film on Pyrex. 46

27 YSZ film on Pyrex (a) (111) pole figure; (b) (220) pole figure. 48

28 (111) pole figures of YSZ films grown on Pyrex with IAD. 49

29 Plan view TEM micrograph and electron diffraction pattern of YSZ film surface. 53

30 Cross-section view TEM micrograph and electron diffraction pattern of YSZ interface. 54

31 SEM (a) plan view and; (b) cross-section view of YSZ film. 56

32 (111) pole figure of specimen prepared by depositing 300 Å without IAD, then turning on the ion beam for 10 min. without YSZ deposition, and then turning the ion beam off until final thickness was reached. 58

33 (111) pole figure of biaxially aligned YSZ film grown with only initial use of IAD. 58

34 XRD pattern of ceria film grown on Pyrex at 600 °C using IAD. 59

35 SEM (a) plan view and; (b) cross-section view of (111) ceria film grown on Pyrex using IAD at 600 °C. 60

36 XRD pattern of (200) oriented ceria film grown using IAD at $\theta = 45°$. 61

37 Rocking curve of (200) oriented ceria film grown using IAD at $\theta = 45°$. 61

38 (111) pole figure of ceria film on Pyrex grown using IAD at $\theta = 45°$. 62

39 SEM (a) plan view and; (b) cross-section view of (200) ceria film grown on Pyrex using IAD at $\theta = 45°$. 64

40 XRD pattern of (111) oriented ceria film grown on soda lime glass using IAD. 65

41 SEM (a) plan view and; (b) cross-section view of (111) ceria film on soda lime glass. 66

42 XRD pattern of (200) oriented ceria film grown using IAD at $\theta = 35°$. 67

43 SEM (a) plan view and; (b) cross-section view of (200) ceria film grown on Pyrex using IAD at $\theta = 35°$. 68

44 (200) biaxial alignment by IAD due to shadowing of misoriented grains. (a) Initial film deposited is polycrystalline; (b) (200) is the fastest growth direction, so these grains ultimately shadow and extinguish the growth of crystallites having orientations other than (200); (c) alignment develops when the net growth of columnar grains varies with respect to the orientation of the ion beam. Columnar grains of a specific orientation will begin to shadow grains which are growing more slowly; (d) this surface roughness induces a growth instability such that the faster growing, biaxially aligned grains begin to dominate the microstructure. 70

ACKNOWLEDGMENTS

I would like to acknowledge the financial support of E-Systems for the ion-beam assisted deposition project and to the Office of Naval Research for my fellowship tenure from September 1989 through August 1992.

I would like to enumerate the three outstanding qualities of my advisor, Prof. Michael Cima, that I will remember the most: 1.) Unmitigated enthusiasm and energy for research, 2.) Insightful solutions for circumventing obstacles in research, 3.) Impressive knowledge of materials science that allows him to determine key experiments. Thanks are extended to Prof. Cima for the time and effort he spent on this project and on my thesis.

I benefited immensely from collaboration on the project with Dr. Neville Sonnenberg, whose expertise enlightened discussions and personality made work most pleasant.

I appreciate the immeasurable support and friendship of Paul McIntyre.

I would like to thank Kevin Ressler for the SEM micrographs, and Paul McIntyre and Ya Ping Liu for the TEM micrographs and electron diffraction results.

Thanks are expressed to Bertha Chang and Paul McIntyre for scientific discussions.

I acknowledge Lenny Rigione and John Centorino for their technical support on the project.

CHAPTER ONE
INTRODUCTION

1.1 Purpose

For high temperature superconducting (HTSC) electronic applications, such as multichip modules (MCM), thin films must be deposited over large areas on substrates that have low dielectric loss. Advantages gained by using superconducting materials in integrated circuits include high density packing of interconnects that fit a greater number of circuits per square centimeter, and microprocessor clock rates in excess of 100 MHz. Low dielectric constant ($\varepsilon < 7$) is an important property for substrate material in superconducting microelectronics because the power dissipation, inductance and capacitance of a substrate are directly proportional to its dielectric constant. The superior electrical performance provided by superconducting circuits will diminish, therefore, if power loss and impedance occurs due to the large dielectric constant of the substrate.

High quality HTSC films ($J_c > 10^6$ A/cm^2 at 77 K) have been successfully deposited on $LaAlO_3$, $SrTiO_3$, MgO, $NdGaO_3$ and yttria stabilized zirconia (YSZ) single crystal substrates. These substrates, however, often are not available in diameters larger than two inches and are too expensive for production. Some single crystal substrates, such as $LaAlO_3$, have large dielectric constants ($\varepsilon = 25$) and are twinned resulting in dielectric anisotropy. Though single crystal MgO is relatively inexpensive, it has dielectric constant of 9.7, is difficult to polish and is mechanically weak [1]. YSZ has become a common single crystal substrate for the growth of BYC [2,3,4,5,6,7] because of its mechanical strength, low cost, and chemical stability. Several recent developments have suggested that non-epitaxial substrates could be used for the preparation of $Ba_2YCu_3O_{6.9}$ (BYC) and other HTSC thin films. YSZ buffer layers were found to produce epitaxial BYC films on Si [8,9] and sapphire [10]. The semiconductor Si, with its dielectric

constant of 12, is not an insulator, of course, making it unsuitable for HTSC MCM applications. In the case of sapphire, its rhombohedral structure causes dielectric anisotropy [11].

BYC must be deposited on substrates with a small dielectric constant for applications such as interconnects and high speed microprocessors. Silicate glasses have dielectric constants between 3.5 and 5.0 at 20 °C, can cover large areas, and are cost effective. Glass, therefore, could serve as an excellent substrate material for HTSC electronics if a method were found to deposit a biaxially aligned buffer layer on the glass to support the subsequent deposition of BYC film. Ion-beam assisted deposition (IAD) is a promising technique for preparing biaxially aligned buffer layers on amorphous substrates. IAD has been used to create biaxially aligned YSZ buffer layers on polycrystalline metal alloy substrates which subsequently could be used to to prepare biaxially aligned BYC films [12,13,14]. Reaction between YSZ and BYC layers may occur that could potentially degrade the superconducting properties of the film for those BYC preparation techniques that employ high deposition temperatures. Cima *et al.* [15] have shown that at 950 °C, YSZ reacts with BYC to form $BaZrO_3$ as a stable end product. The appearance of $BaZrO_3$ as an interfacial layer between YSZ and BYC was also detected by Tietz *et al.* [4]. Other materials for biaxially aligned buffer layers, such as CeO_2, should also be investigated since an interfacial reaction may occur with YSZ. BYC deposited on a CeO_2 buffer layer on single crystal $LaAlO_3$ produced high quality superconducting film ($J_c > 10^6$ A/cm^2 at 77 K) [16].

The purpose of this thesis is to demonstrate the growth of biaxially aligned, cubic, (200) oriented YSZ and CeO_2 buffer layers on glass substrates using IAD for eventual application in HTSC electronics. The microstructure and orientation of the dielectric films produced by IAD experiments will be characterized, and the parameters for deposition will be determined. A model for the growth of the biaxially aligned dielectric

films on amorphous substrates using low engery ion bombardment will be developed from the experiments performed.

1.2 Microstructural Models for Evaporated Films

The microstructure of a thick film is ultimately influenced by the early stages of film nucleation and growth. Movchan and Demchishin [17] discussed the dependence of microstructural development in films on the substrate temperature expressed as a fraction of the melting temperature (T/T_m) in Kelvin. Thorton [18] expanded the model for films deposited by sputtering to include the effects of gas pressure. Thorton examined the effects of structure on the mechanical properties of film and reviewed microstructural development concepts for film growth by physical vapor deposition. The structure zone diagram in Figure 1 expresses the relationship between processing conditions and microstructure. The diagram illustrates how surface topography and microstructure vary with Ar pressure used during sputtering and substrate temperature, which is expressed as a fraction of the absolute melting point. Zone 1 ($T/T_m < 0.25\text{-}0.3$) is characterized by tapered crystallites that have voids along the grain boundaries with domed tops and poor mechanical strength. The Zone 1 microstructure results when adatom diffusivity is not large enough to overcome the effects of atomic self shadowing. Shadowing produces voids, especially when vapor atoms arrive from an oblique angle, because higher points on the film surface receive more flux than lower points [19]. Surface roughness may occur from preferential nucleations on substrate inhomogeneities or substrate roughness. The transition microstructures in Zone T are also dominated by shadowing effects, but appear to have finer, fibrous grains with greater mechanical strength. Zone 2 ($0.25\text{-}0.3 < T/T_m < 0.5$) is comprised of smooth topped granular structures which are controlled by adatom surface diffusion processes. The columnar microstructure has smooth surface facets and good mechanical integrity at the grain boundaries. The polyhedral structure of the equiaxial crystallites characteristic of Zone 3 ($T/T_m > 0.5$) are dominated by bulk

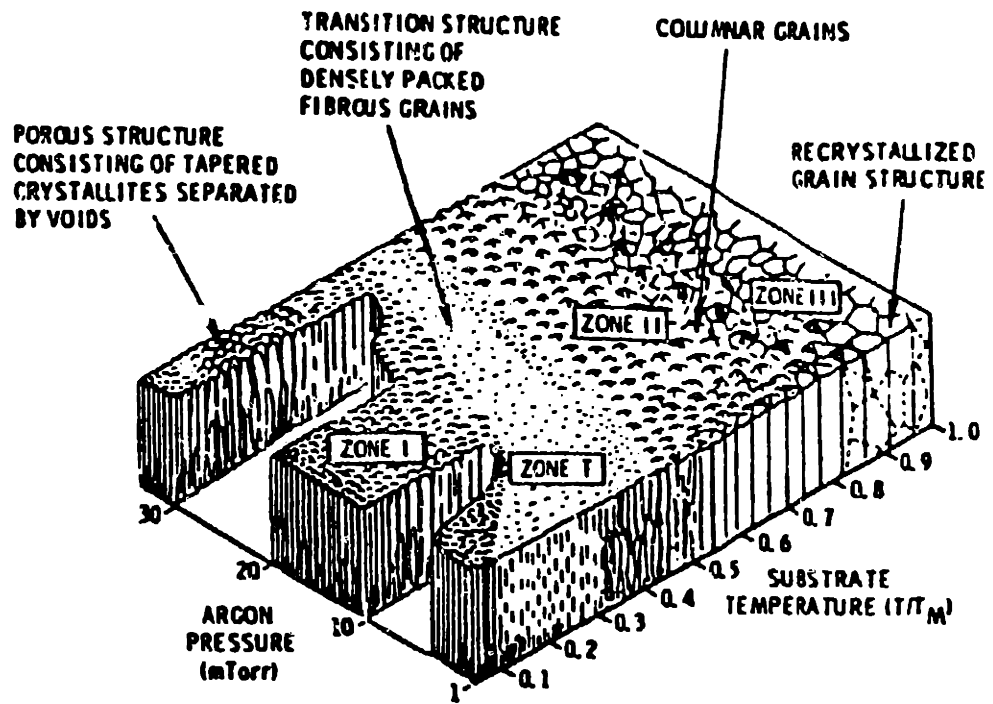

Figure 1. The three dimensional zone structure model by Thorton [18].

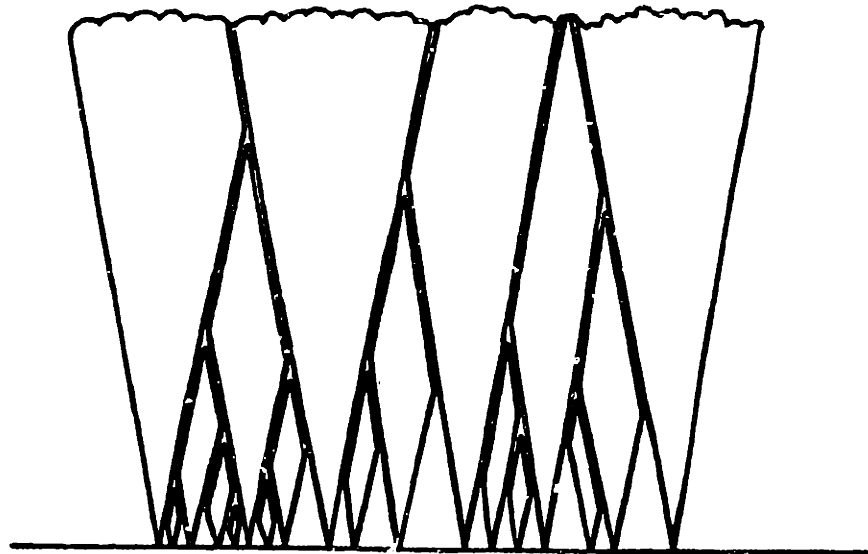

Figure 2. Growth-death competition in conical column evolution [21].

diffusional processes. In the Zone 3 temperature regime, recrystallization and surface reconstruction commonly occur from the minimization of surface energy and strain energy so that columnar grains recrystallize to form the equiaxial grains.

Alternative models have been proposed to explain the evolution of these different microstructural zones. Grovenor et al. [20] suggests that Zone 1 microstructure is dependent on the critical nucleus size of a grain at low temperature, and at higher temperatures the evolution of the columnar microstructure is due to the increasing mobilities of grain boundaries. Messier [21], however, describes columnar growth as the self organization of structures competing for maximum cone growth as shown in Figure 2. The conical columns evolve from a death-growth competition in which the columnar density is determined by the size distribution of clusters nucleating on the surface. The microstructural zone model illustrates the strong dependence of film structure on substrate temperature and other processing parameters regardless of its specific interpretation.

1.3 Nucleation Model for Low Energy Ion Bombardment

Low energy ion bombardment during evaporation can lead to extensive changes in the physical properties of films including the modification of grain size, film density and voids, the direction and degree of orientation, and mechanical stress [22-26]. The mechanisms reponsible for film modification due to low energy ion irradiation are complex and include various ion induced processes, such as adsorption sites due to defect production on surface, collisionally stimulated dissociative chemisorption, ion induced chemical desorption, recoil implantation, trapping, collisional mixing, preferential sputtering, change in segregation behavior, local electrical effects from charging, and enhanced adatom diffusion [27]. Ion induced processes have been used to model and interpret results of experiments that determine the effects of low energy ion bombardment on nucleation and growth kinetics.

Ion bombardment during nucleation can create nucleation sites and changes in the nucleation rate as shown by Kirkorian and Sneed [28] in the growth of Ge films. The number of ion induced nucleation sites can be determined from the difference between the rate they are generated, which is a function of the ion current density, the beam energy, and the mass and chemistry of the incident species, and the rate the sites are lost, which is lagrely dependent on surface energy due to substrate temperature. A decrease in the number density and size of island nucleation in the presence of ion bombardment for a nominal film thickness has been reported by Marinov [29] and Hasan *et al.* [30,31]. A mechanism Hasan *et al.* [30] proposed for the larger average island size in systems where the adatom and substrate are only weakly bound is the depletion of small clusters by ion induced dissociation and sputtering. The smaller the size of the clusters, the greater their surface mobility, and they diffuse to aid in the coarsening of larger, stable islands. For small clusters which are reduced to subcritical size, the change in free energy favors spontaneous dissociation into adatoms which either desorb from the surface or contribute to the coarsening of large clusters. The large islands, however, seem only to lose a minor amount of material due to sputtering from ion bombardment. These effects are most likely to occur when deposition conditions favor high nucleation rates and when the ratio of ions to atoms is large.

Hasan *et al.* [30] conducted experiments to test this mechanism in which In islands were vapor deposited on amorphous Si_3N_4 substrates to nominal thicknesses of 15 Å and 100 Å. Thermal In and partially ionized In^+ beams, having an ion to neutral atom ratio of 0.35, were provided by an ultrahigh vacuum, metal ion source which generated low energy ion beams of 0 (thermal), 150, 200, and 300 eV. The flux of the thermal In was $3.0x10^{13}$ atoms/cm²s, and the total ion flux was $4.6x10^{13}$ atoms/cm²s. Substrates were heated to 30 °C making the deposition temperature less than the 117 °C melting temperature of In. The island size distribution, distance between the islands, and island

number density were reported as a function of ion beam energy and nominal film thickness. TEM micrographs of the deposited In films are shown in Figure 3. Ion bombardment clearly resulted in larger average island sizes for for a given film thickness. For 100 Å thick films the final average island size increased with beam energy. The average island diameter was 6.5 nm for thermally deposited In, 8 nm when the beam energy was 150 eV, 13 nm for 200 eV ions, and 50 nm when the beam energy was 300 eV. Figure 3 also reveals the decrease in secondary nucleation with higher beam energies until at 300 eV, virtually no island was observed to have a diameter of less than 11 nm. Indium film was subsequently deposited without the ion beam on top of the fractional monolayer of film predeposited with In^+ ions. The In film developed the same island size distribution on the bare patches of substrate between the predeposited islands as occurred for the thermally grown films on clean substrates. The evidence suggests, therefore, that for this case ion bombardment produced no preferential nucleation sites.

The decrease in the secondary nucleation rate and the increase in the average island size were attributed to the depletion of small clusters which diffused to feed the larger islands, as previously discussed. Ion bombardment gives rise to increased adatom diffusivity at relatively small deposition rates and for weakly interacting systems like In on Si_3N_4. The regions between the islands were undersaturated and ion bombardment created larger, island capture cross-sections. Surface diffusion continued to dominate island growth even for 100 Å thick films for experiments using In^+ bombardment. The observed nonuniformity in the island size distribution was due to the strong influence of coalescence among small islands, however, for thermal deposition.

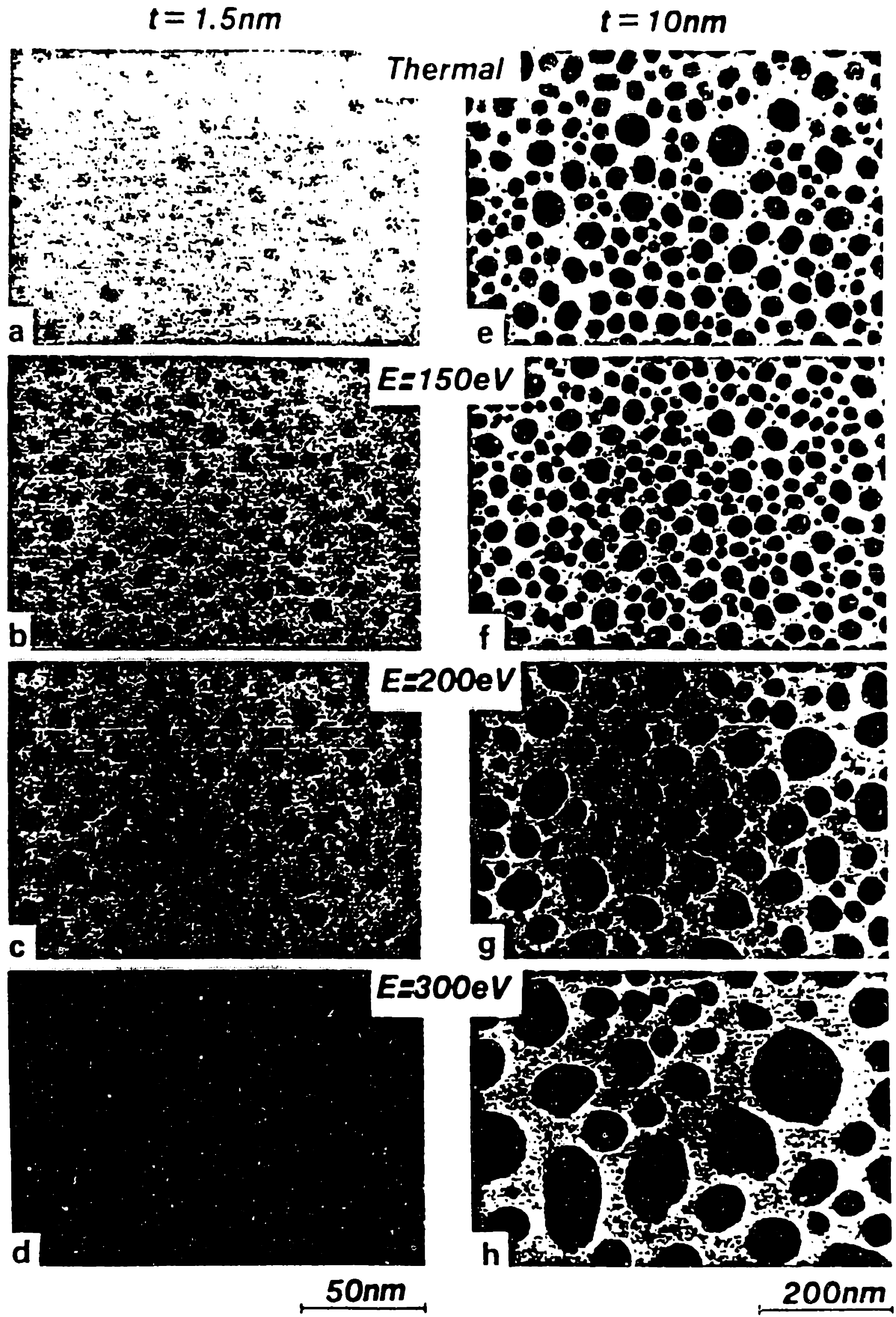

Figure 3. TEM micrographs showing island size and density for In deposited on Si_3N_4 [30].

CHAPTER TWO
REVIEW OF RELATED WORK

2.1 Ion-beam Assisted Deposition of Zirconia Films

Martin *et al.* [32,33] used normal incidence IAD to grow ZrO_2 films on glass substrates for optical characterization. The 99% pure ZrO_2 source was deposited by e-beam evaporation to a thickness of 1 μm on substrates made from micrcosope glass slides at a rate of 8 Å/s. Oxygen and argon were used separately as ion source gases bringing the deposition pressure to 0.75×10^{-4} Torr. The ion current density was 200 μ A/cm^2, and the beam energies were 600 eV for argon and 1200 eV for oxygen. A series of experiments were conducted in which ZrO_2 films were grown with and without IAD on substrates which were either held at room temperature or heated to 300 °C. The XRD patterns for films produced without IAD are shown in Figure 4 indicating the monoclinic phase predominated for ZrO_2 deposited at 300 °C, but the film was amorphous when deposited at room temperature. Figure 4 indicates that the XRD patterns of films deposited at 300 °C remain monoclinic when both oxygen and argon gas sources were used for IAD. IAD during room temperature deposition, however, had the effect of creating the cubic phase in ZrO_2 films contrasting the amorphous film deposited without IAD.

Martin *et al.* [32] performed experiments to determine the impact on the microstructure of the ZrO_2 film caused by turning the oxygen ion beam off during half of the deposition. The top half of the ZrO_2 film had the columnar microstructure when deposited with IAD, but the bottom layer grew fully dense after the oxygen ions were switched off midway through the run. When the oxygen ions were switched on only after the deposition was halfway to completion, the opposite occurred. A dense top layer of ZrO_2 film covered voids in the columnar structure beneath. These experiments indicate that the ion bombardment provided enough energy to disrupt the columnar

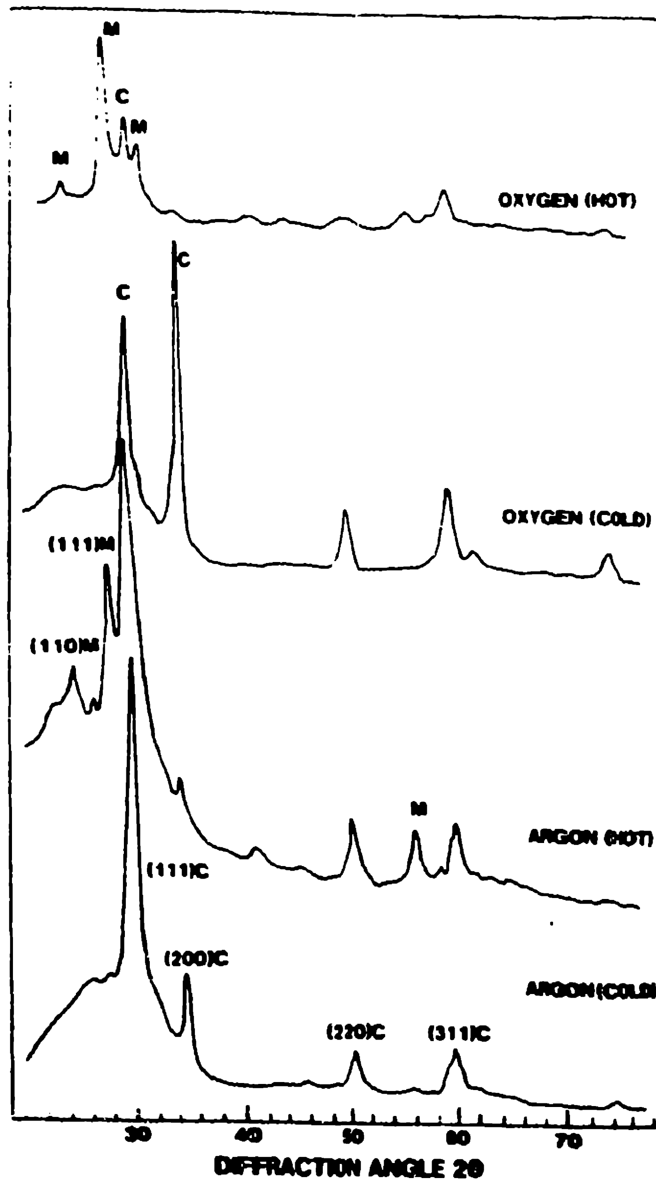

Figure 4. XRD patterns of zirconia film grown on 300 °C (hot) and ~20 °C (cold) glass substrates with IAD using either argon or oxygen source gases [32].

growth [32], so that the densification works as a growth phenomenon and occurs independent of either deposition surface.

2.2 Ion-beam Assisted Deposition of Ceria Films

Ceria is an important oxide material for use in high index films and optical devices because of its large refractive index (n ~ 2) and good transmission in the visible and near infrared regions of the spectrum [34]. Literature pertaining to the growth of CeO_2 films by ion assisted deposition focuses on optical applications and, therefore, emphasize the effects of deposition parameters on film density and refractive index. Al-Robaee *et al.* [35,36] report that CeO_2 films were deposited using IAD on optically polished fused silica substrates. The CeO_2 source material was deposited by e-beam evaporation at a rate of 3 Å/s to a thickness of 0.25 - 0.35 μm. Either neutral or ionized oxygen was supplied to the chamber causing a deposition pressure of 0.7×10^{-4} Torr.

Sputtering yield anisotropy for single crystal oxides has not been studied in detail, but the modification of film microstructure by IAD has been reported. Al-Robaee *et al.* [35,36] examined structural properties with X-ray diffraction (XRD) 2θ scans in three series of experiments relating the film orientation to substrate temperature, the presence of ionized or neutral oxygen, and the ion beam energy. Their results showed that the normal orientation of CeO_2 crystallites was significantly modified by ion beam bombardment. The XRD patterns shown in Figures 5 and 6 exhibit a mixture of (111), (220), and (311) orientations in the films, but do not indicate any (h00) orientation. No information, however, was provided on the in-plane orientation of the films. The first study compares CeO_2 films grown with and without IAD. Substrate temperatures ranged from room temperature to 300 °C, and the oxygen ion beam had a current density of 220 μA/cm² and an ion energy of 600 eV. Without IAD, however, the (220) orientation becomes nearly as strong as the (111) at 300 °C. In a different study, Al-Robaee *et al.* [36] examined the effect of ion beam energy on film orientation. The beam

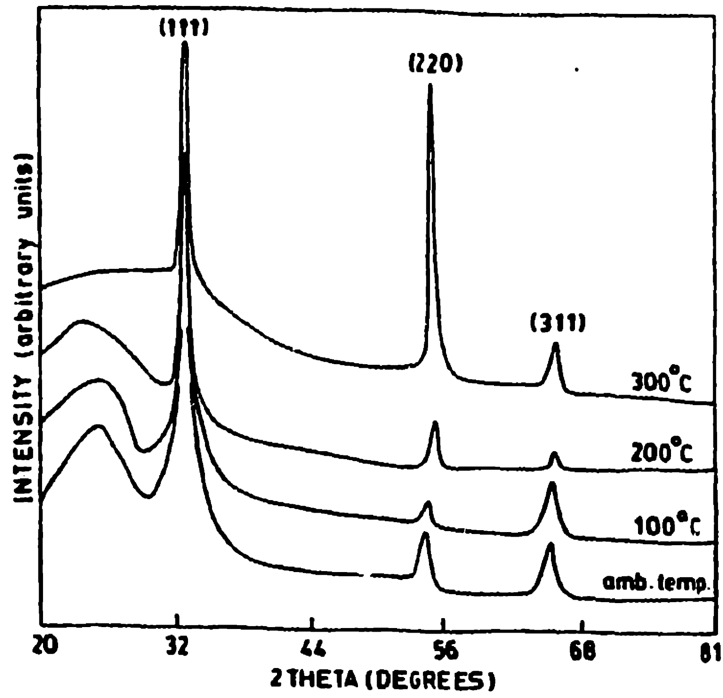

Figure 5. XRD patterns of zirconia films grown without IAD at different substrate temperatures [35].

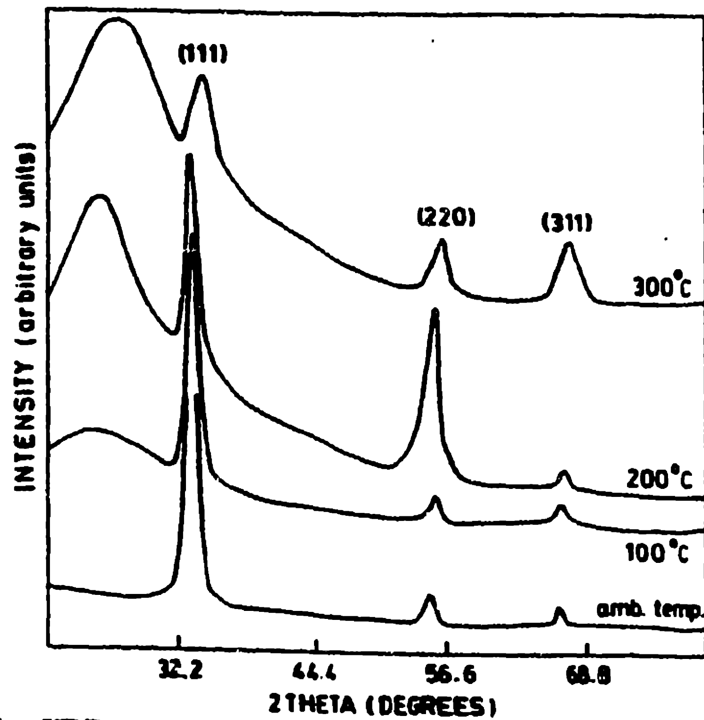

Figure 6. XRD patterns of zirconia films grown with IAD at different substrate temperatures [35].

energies ranged from 300 - 700 eV while the ion current density was 220 μA/cm^2, and the temperature was 300 °C. The XRD patterns in Figure 7 show that the (111) orientation was strongest at the lower beam energies, but the (220) grows with respect to the (111) as the beam energy was increased until at 700 eV, the (220) and (111) peaks are nearly equal in magnitude.

Netterfield *et al.* [37] reported similar results for CeO_2 films deposited on optically polished borosilicate crown glass substrates using normal incidence IAD. The CeO_2 was deposited by e-beam evaporation at a rate of 2.0 Å/s to a thickness of 1 μm. Films were prepared with and without IAD and deposited on both unheated substrates and substrates heated to 300 °C. The authors did not mention whether oxygen was present in the chamber in the experiments without IAD. The oxygen ion current density was 160 μA/cm^2 with a beam energy of 1.2 keV. Netterfield *et al.* reported oxygen implantation due to a beam energy larger than 1.0 keV. The relative intensities of the cubic (111) and (220) XRD peaks are shown in Figure 8 for this study. The ratio between the intensities of the (111) and (220) peaks were similar for films grown both with and without IAD, but for unheated substrates the (111) orientation was more pronounced. At 300 °C, IAD had a marked effect on orientation; without IAD the films were strongly (111), but in the presence of oxygen ions, the (220) orientation predominated.

The beam energies and ion current densities of IAD experiments conducted by Al-Robaee *et al.* and Netterfield *et al.* often exceeded those used in this theses by an order of magnitude since their purpose was to grow dense CeO_2 films for optical applications. Films grown at 300 °C without IAD or at beam energies less than 600 eV are not fully dense and have the columnar microstructure [35,37]. Netterfield *et al.* [37] proposed that at 50-100 eV, ions do not transfer the energy required to increase their surface mobility enough to overcome the effects of atomic self-shadowing that enables the growth of the columnar microstructure typically observed in evaporated dielectric films.

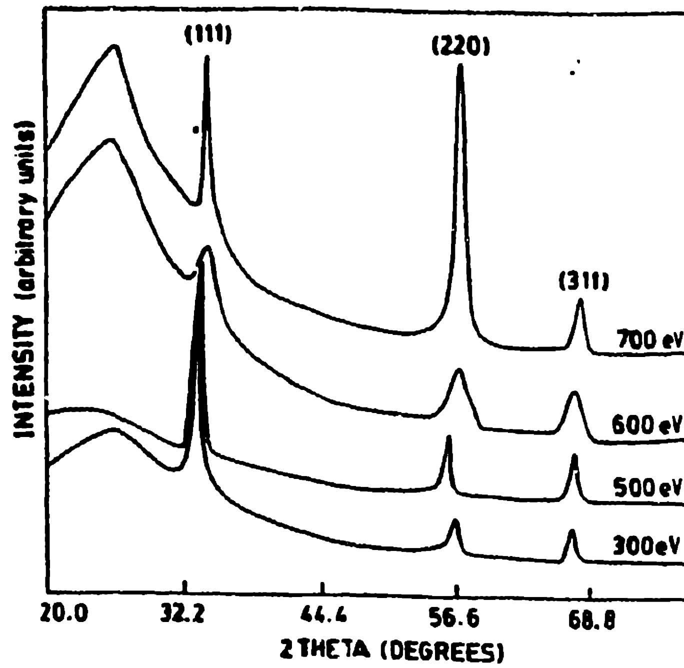

Figure 7. XRD patterns of zirconia films grown with IAD at different ion beam energies [35].

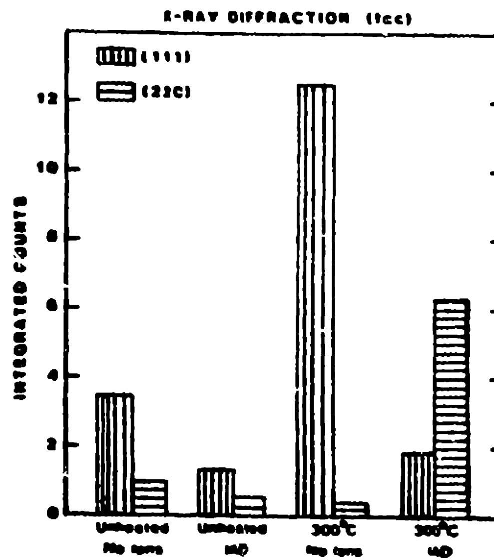

Figure 8. Integrated counts for (111) and (220) XRD peaks in ceria films grown using IAD [37].

2.3 Growth Model for IAD of Ceria and Zirconia Films

Muller [38] has proposed the mechanisms for ion induced densification of the Zone 1 films classified by the Thorton model as discussed above. Muller performed Monte Carlo simulations of the growth of ZrO_2 films by IAD using O^+ ions arriving at an angle 30° from normal to the substrate and having beam energies of 600 eV. Muller asserted that ions penetrate the surface of a porous film to a depth of only a few interatomic spacings. The interacting ions produce vacancies and phonons, displace atoms and create electronic excitations. Ions in the model are either incorporated or backscattered, while displaced atons may leave the surface through sputtering or may be forced deeper into the film where they may be trapped as interstitials or moved into vacant sites. Vacancies produced by ion bombardment near the surface of the film are at least partially refilled by newly arriving adatoms. Figure 9 illustrates the densification process occuring when ion bombardment and vapor arrival are treated as alternating events. The refilling of ion induced vacancies results in the downward packing of atoms when the ion to atom ratio is sufficiently large, so that the film no longer grows with a porous, columnar microstructure, but instead is densely packed. Muller compared his theoretical results for film density as a function of ion to atom ratio with experimental results from Martin *et al.* [32]. Figure 10 shows that simulated and experimental results correlate for low ion to atom ratios as the films are columnar and not fully dense.

Martin and Netterfield [39] compared the densities of CeO_2 films grown using IAD with O^+ ions arriving at an angle of 30° from normal to the substrate and having energies of 25, 150, and 600 eV. Figure 11 shows film density as a function of ion to atom ratio and beam energy. The experimental results agree with the theoretical molecular dynamic calculations performed by Muller. Films deposited when the beam energy is 150 eV exhibited the most densification. The Monte Carlo simulations suggest that the cross section for atom displacement is low due to sputtering and atomic recoils for beam

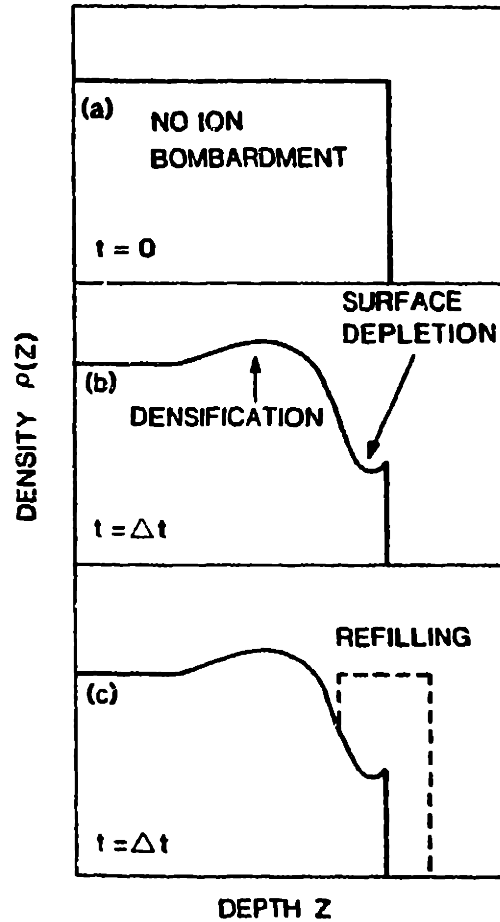

Figure 9. Film density distribution (a) without IAD, given an abrupt decrease in density at the surface; (b) after a period of ion bombardment; (c) condensing vapor refills the depleted surface region without IAD [39].

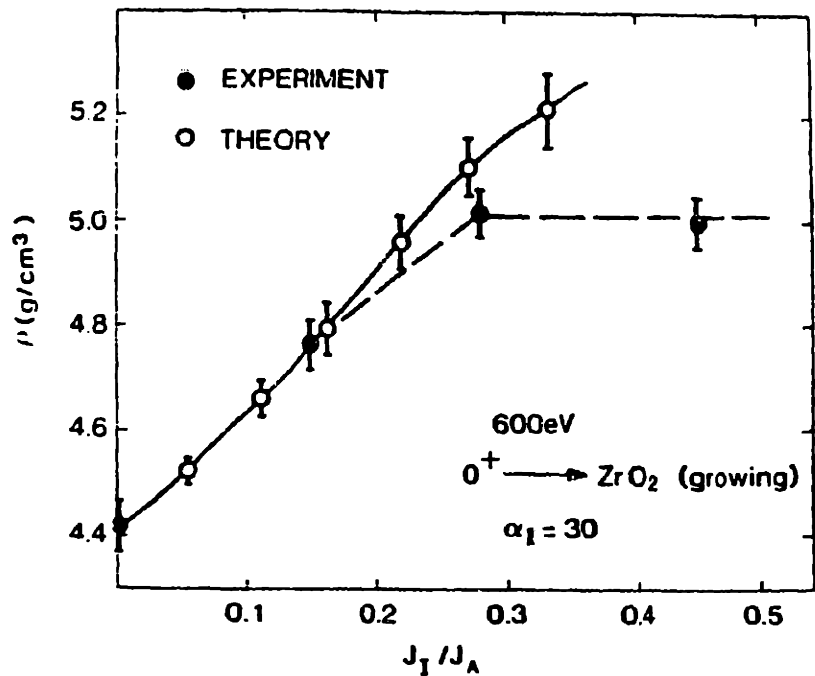

Figure 10. Density as a function of the ion-to-atom arrival rate for zirconia films grown using IAD [32].

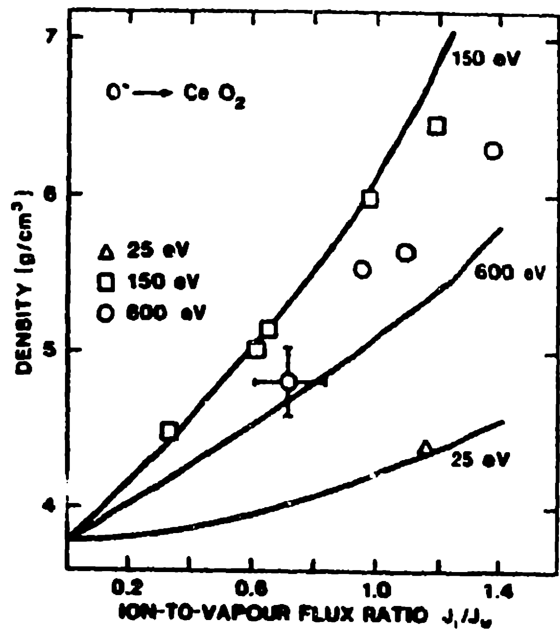

Figure 11. Experimental and theoretical density as a function of the ion-to-atom arrival rate for ceria films grown using IAD [38].

energies as low as 25 eV. Conversely, at 600 eV vacancies are created beneath the surface of the film. The refilling depth for atomic vapor is between one and two atomic diameters so the incoming vapor does not have a path to fill the vacancies.

2.4 Effect of the Angle of Ion Incidence on Channeling in Metal Films

Ion bombardment of thin films can cause significant changes in microstructure as described above, but the effects of ion channeling can be studied by varying the angle of ion incidence in separate IAD experiments. Dobrev [40] and Van Wyk and Smith [41] independently correlated texture development in polycrystalline films with the ion channeling direction. Van Wyk [42] demonstrated that when copper film was bombarded after deposition with an off-normal incidence ion beam of 40 keV Cu ions, preferred orientation resulted in the direction of the ion beam. Sputtered or vapor deposited copper is (111) oriented without IAD. A (110) fiber texture resulted normal to the surface of the film when normal incidence ions were used. The (110) orientation still formed when off-normal incidence was employed, but the (110) axis was parallel to the direction of the ion beam. Channeling in fcc materials is most pronounced in the (110) direction, followed by the (100) and (111) directions. The alignment of (110) planes in the direction of the ion beam in copper films, therefore, was explained as a channeling phenomenon for high energy ions [43].

The effect that low energy, off-normal incidence ion bombardment applied during deposition has on crystal structure was examined by Yu *et al.* [44,45,46] for niobium films sputter-depsited on fused silica substrates at room temperature. A 200 eV Ar^+ ion beam bombarded the surface during deposition at 20° from parallel to the substrate. A strong (110) fiber texture was formed without IAD in which the crystallographic axis was pointed perpendicular to the plane of the substrate as shown by the Schultz X-ray pole figure in Figure 12. The ring surrounding the central spot corresponds to diffraction from the (110) planes that are 60° from parallel to the substrate. The uniform

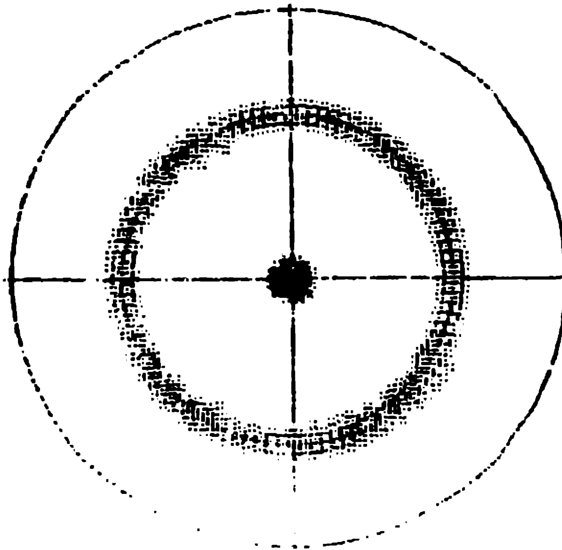

Figure 12. (110) pole figure of Nb film grown without IAD [44].

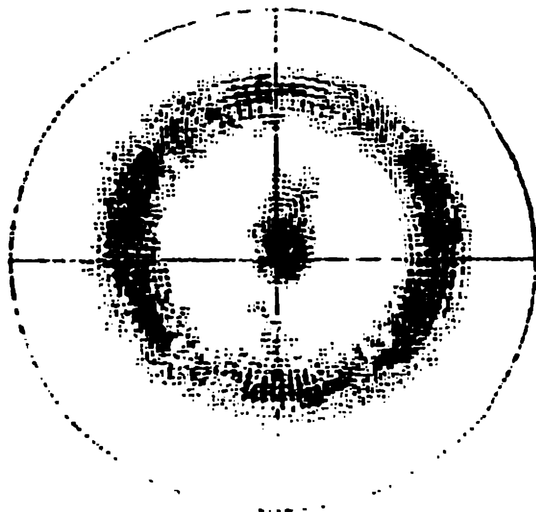

Figure 13. (110) pole figure of Nb film grown with IAD [44].

intensity of the ring indicates that the crystallites were randomly oriented in the azimuthal plane. The (110) fiber texture usually is found in vapor deposited or sputtered bcc thin films, such as niobium, but the (111) fiber texture is common for copper and other fcc metals, as previously described [43].

The azimuthal distribution of crystallites in the film was modified when the Nb film was prepared with off-normal incidence ion bombardment during growth, as the pole figure in Figure 13 reveals. The continued presence of fiber texture is indicated by the strong central peak, however, the intensity of the 60° ring is no longer uniform. The direction of the ion beam goes from the top to the bottom of the figure so that the incident ions lie in a planar channeling direction between the (110) planes. The evidence for some azimuthal orientation from the pole figures was confirmed by nonuniform rings displayed in TEM diffraction patterns [46] obtained from thinned films. The degree to which the film is oriented was computed by taking the ratio of the intensity of the XRD maxima on the ring at 60° to the intensity of the central peak. The results, shown in Figure 14, indicate that the degree of orientation increased with the arriving ion flux. Approximately half of the crystallites were aligned to within 5° of a channeling direction when the ion to atom arrival ratio was 1.3. About ¾ of the arriving Nb atoms were supposedly resputtered for these ion bombardment parameters [43].

The ion penetration depth should only be several Angstroms for the low ion energies used in these experiments. Bradley *et al.* [47] have proposed a theory for the orientation of thin films during deposition by off-normal incidence ion bombardment. The suggested mechanism is based on variation of sputtering yield with ion beam orientation for single crystal targets. The development of a textured microstructure is thought to be the result of the higher sputtering yields of all orientations other than the channeling direction. Thus, carefully balancing the deposition rate and the ion induced sputtering would cause a net deposition of those crystallites oriented in the low sputtering yield direction.

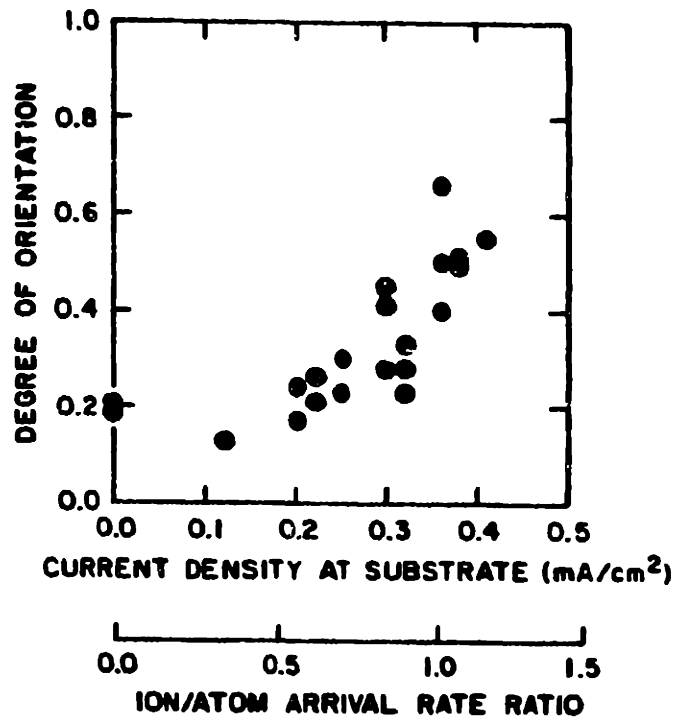

Figure 14. Degree of orientation of Nb films as a function of the ion-to-atom arrival rate during deposition [44].

Bradley [43] suggested that Yu *et al.* [44,45,46] should have used an ion bombardment angle of 45° because channeling in the (100) direction would align (100) oriented crystallites in the direction of the beam creating (110) azimuthal orientation perpendicular to the substrate surface. Bradley also remarked that since large atoms do not channel well, to optimize channeling, the smallest specie of ion that does not chemically react with the substrate should be used. Argon was used as the major ionization source gas for IAD experiments detailed in this thesis. Perhaps channeling effects would have been even more pronounced in the resulting dielectric films if a lighter source gas, such as He, was used.

2.5 IAD of YSZ Films on Polycrystalline Substrates

Ion-beam assisted deposition (IAD) has been used to create biaxially aligned buffer layers on polycrystalline substrates which later can be used to prepare biaxially aligned HTSC films. Iijima *et al.* [12,13] reported the preparation of biaxially aligned YSZ thin films on Ni-based Hastelloy substrates using dual ion beam deposition. The XRD pattern in Figure 15 exhibits the (200) oriented YSZ film. The bombardment angle of the substrates was optimized at $\theta = 45°$ to maximize the degree of in-plane alignment of the film. The (111) pole figure shown in Figure 16, reveals biaxially aligned YSZ film which is oriented so that one of the (111) axes in the figure is aligned with the direction of the incident ion beam. Subsequent deposition of BYC, by laser ablation, produced films with critical current densities of 2.5×10^5 A/cm^2 (77K, 0T) which decayed only slightly with applied field. Biaxially aligned YSZ films on a metal wire were somewhat less successful for the growth of BYC films by CVD [48]. The critical current density of these films was 7.4×10^4 A/cm^2 (77K, 0T).

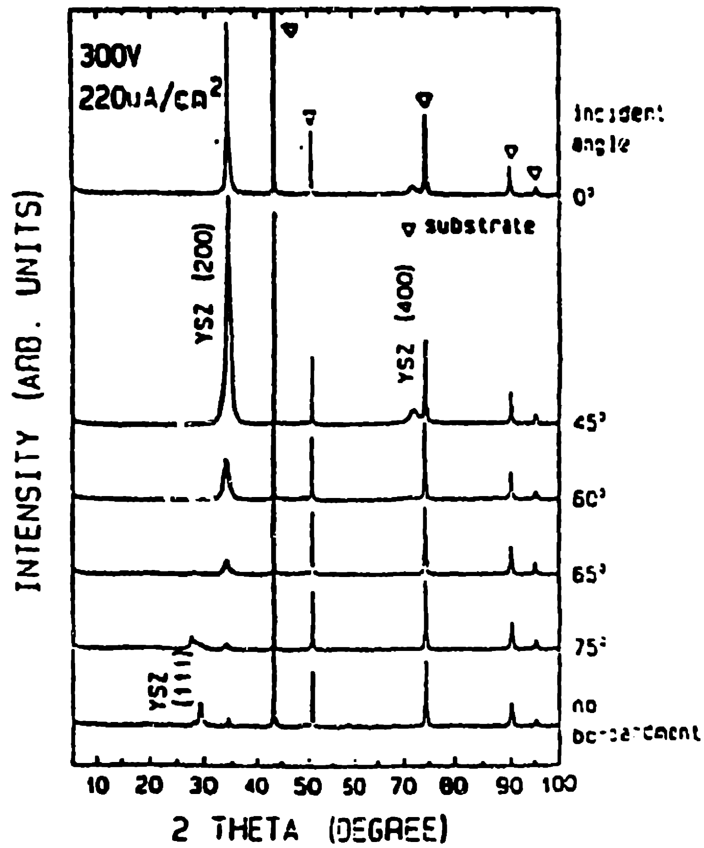

Figure 15. XRD patterns of YSZ films grown on Hastelloy using IAD [12].

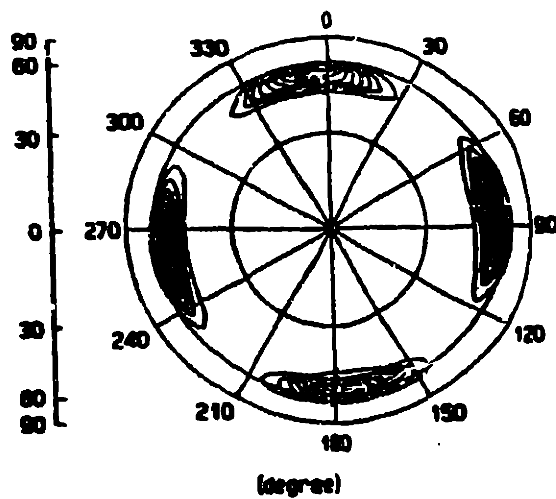

Figure 16. (111) pole figure of YSZ film grown on Hastelloy using IAD [13].

Reade *et al.* [14] have recently deposited YSZ on polycrystalline metal alloy substrates at 70° C to 150° C using ion assisted pulsed laser deposition. Figure 17 shows XRD patterns for YSZ films and indicates enhancement of the (200) orientation due to ion-beam assistance. The biaxial alignment occurred when argon was used as the ion source gas as the (111) ϕ-scan in Figure 18 reveals, but the authors did not report the direction of ion bombardment with respect to ϕ-scan peaks. No biaxial alignment was observed, however, when the source gas was oxygen. They attribute the different effects of the two ions to the inertness of argon and to the differences in size and mass between oxygen and argon ions. Changes in ion beam current were not found to affect the in-plane texture, although changes in the ion voltage were found to play an important role. No biaxial alignment was observed at low voltages (<50 V), while higher voltages (~200 V) increased texture. BYC films deposited on the buffer layer had the following properties: T_c = 92K and $J_c = 6x10^5$ A/cm^2 (77K, 0T) and $J_c = 8x10^4$ A/cm^2 (77K, 0.4T).

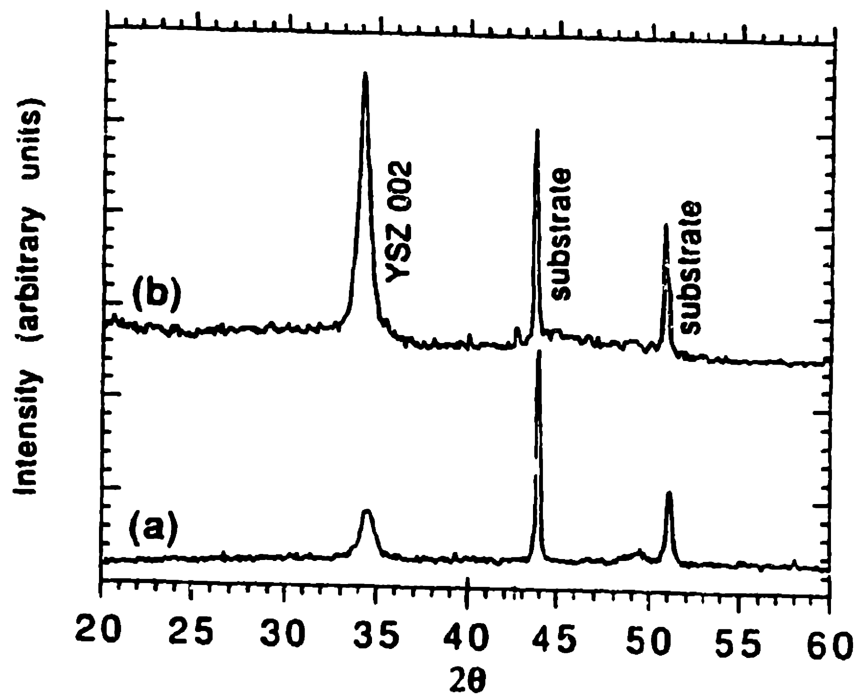

Figure 17. XRD patterns of YSZ films grown on Haynes Alloy (a) with and; (b) without IAD [14].

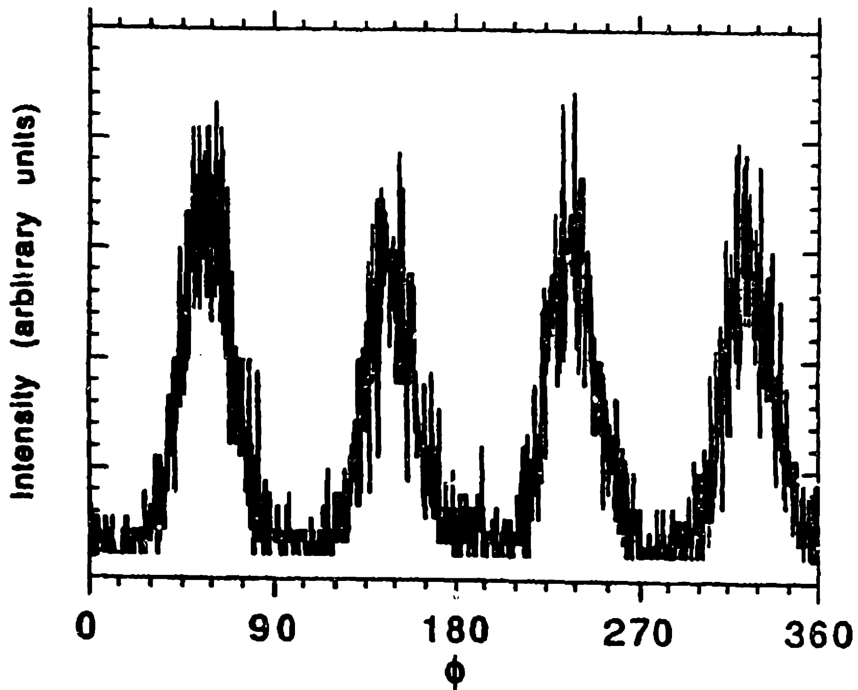

Figure 18. (111) ϕ-scan of YSZ grown on Haynes Alloy with IAD [14].

CHAPTER THREE
EXPERIMENTAL PROCEDURES

3.1 Experimental Apparatus

A schematic diagram of the IAD apparatus is shown in Figure 19. The system consists of an ion beam source and a standard e-beam evaporator. The source material was evaporated from a multiturret, water cooled, copper crucible using a Temescal (Berkeley, CA) 14 kW electron gun with specimen sweep capability. A diffusion pump provided a background pressure of 2×10^{-7} Torr prior to gas flow through the ion source. The electrodes leading to the electron gun were encased in quartz glass tubing to eliminate electrical arcing that could be induced from the plasma generated by the ion source during deposition. A vertical shield was placed between the ion source and the evaporation source to protect the ion source from the dielectric as it is deposited. The Ion Tech 3RF-1200-100 ion source (Ion Tech, Inc., Ft. Collins, CO) provided a 3 cm diameter beam. The rf ion source, shown in the diagram in Figure 20, ionizes the gas stream through inductive coupling of rf power to the ion source discharge chamber. The voltages across the beam and accelerator grids have opposite polarity to first attract the ions from the body of the discharge chamber and then propell them out into the vacuum chamber. A plasma bridge neutralizer (PBN) supplies electrons to the positively charged ion beam creating a net neutral conducting plasma. A net neutral plasma is desired so that the ions are not deflected from their path to the substrates by charged surfaces within the vacuum chamber.

The angle θ between the plane of the substrate and the ion beam could be varied by adjusting the mounting block support mechanism. The ion source was fixed vertically in the vacuum chamber so that the ion beam was emitted directly below the mounting block. The bombardment angle between the ion source and the substrates was varied from 8° to 63° in the experiments reported here. This angle θ differs from that reported

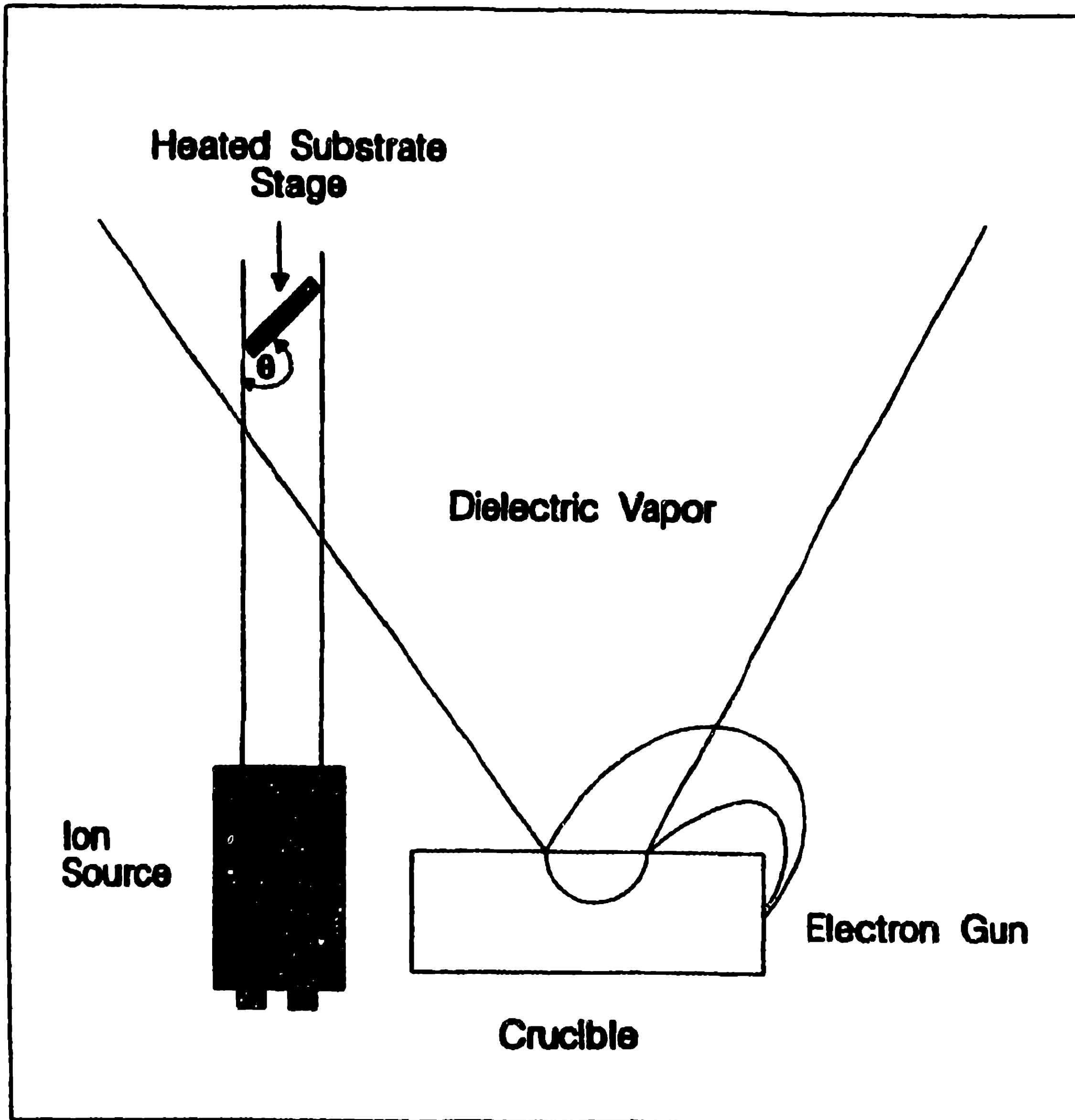

Figure 19. Schematic of ion-beam assisted deposition system.

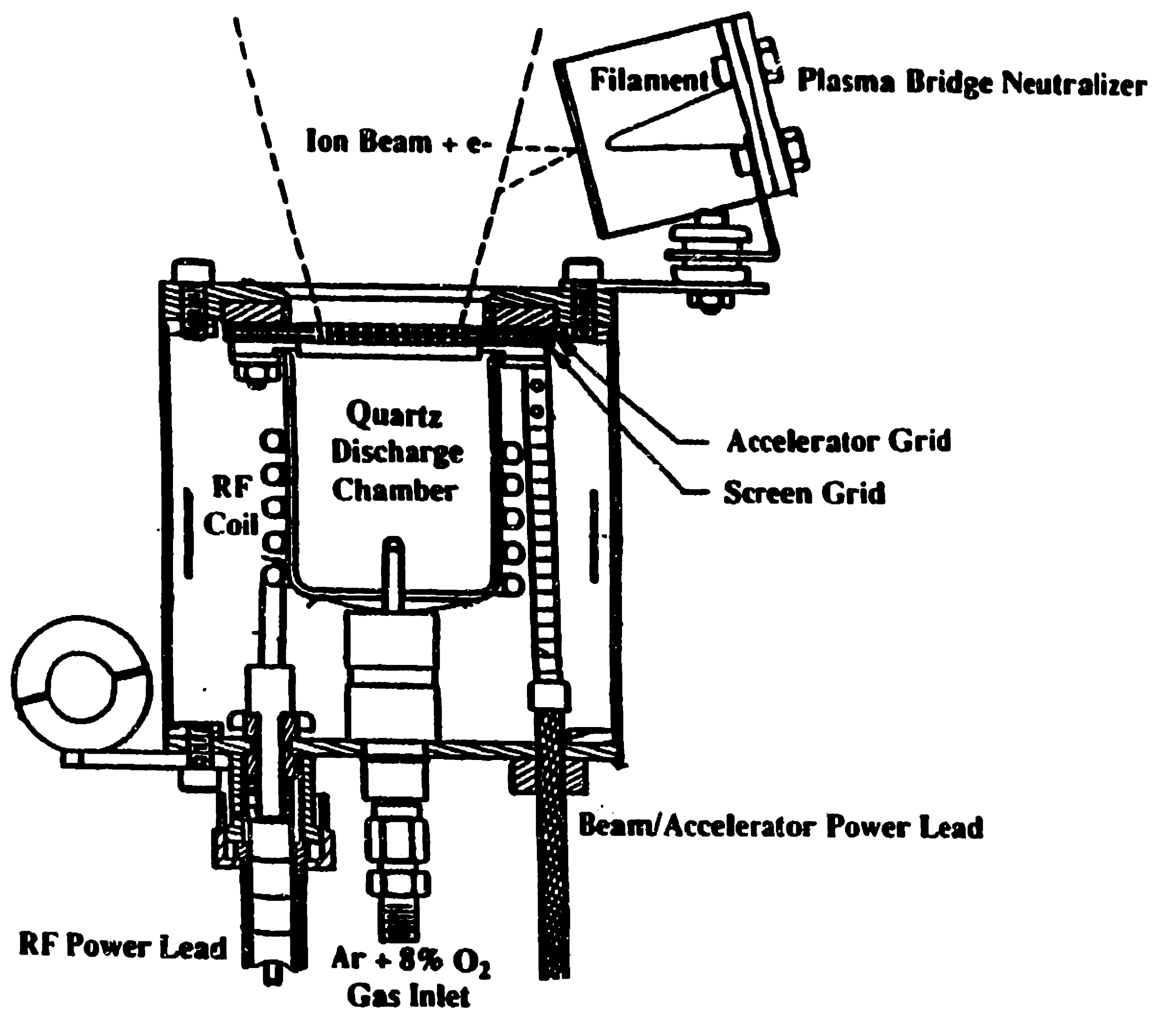

Figure 20. Schematic of Ion Tech 3RF-1200-100 ion source.

by Iijima *et al.* [12,13] by the complement of 90° since they reported the angle between the ion beam and the normal to the substrate.

3.2 Substrate Mounting

Substrates were attached to the mounting block with thermally conducting silver paste (SPI Supplies, West Chester, PA). Thermal contact between the substrates and the mounting block was critical. Poor thermal contact meant lower temperature at the substrate surface and often resulted in the deposition of dielectric films which did not have the (200) orientation. Before mounting the substrates, the blocks were polished using Noxon 7 (Boyle-Midway, N.Y., NY) and a Scotch-Brite (3M, St. Paul, MN) and ultrasonicated in acetone to remove any residue. The substrates were cleaned by consecutively ultrasonicating them in trichloroethane and acetone.

A thin layer of silver paste was squeezed onto the cleaned mounting block and smoothed with a wooden applicator. Smoothing the layer of paste made it uniformly thick and uniformly mixed as the binder and silver may separate. The substrates were placed on the paste and pressed with the end of the wooden applicator to remove trapped air. A curing profile for the silver paste, shown in Figure 21, was developed based on the procedure used by Westerheim [49]. Components of the organic-based binder in the paste were found to volatilize near three different temperatures: 80 °C, 220 °C, and 400 °C. The mounted substrates were placed in a drying oven for the initial bake out at 80 °C for 3 hours. The silver paste was still pliable upon removal, and the end of the wooden applicator was used to press out any air that became trapped beneath the substrate when a portion of the solvent volatilized. The substrates were transferred to a Nytech 85P furnace (Barkmeyer Div., Ney, Yucaipa, CA) for the high temperature bake out and ramped at a rate of 1 C°/min. in air to a temperature of 220 °C at which they were held for 4 hours. The substrates were then taken to 400 °C at the same ramp

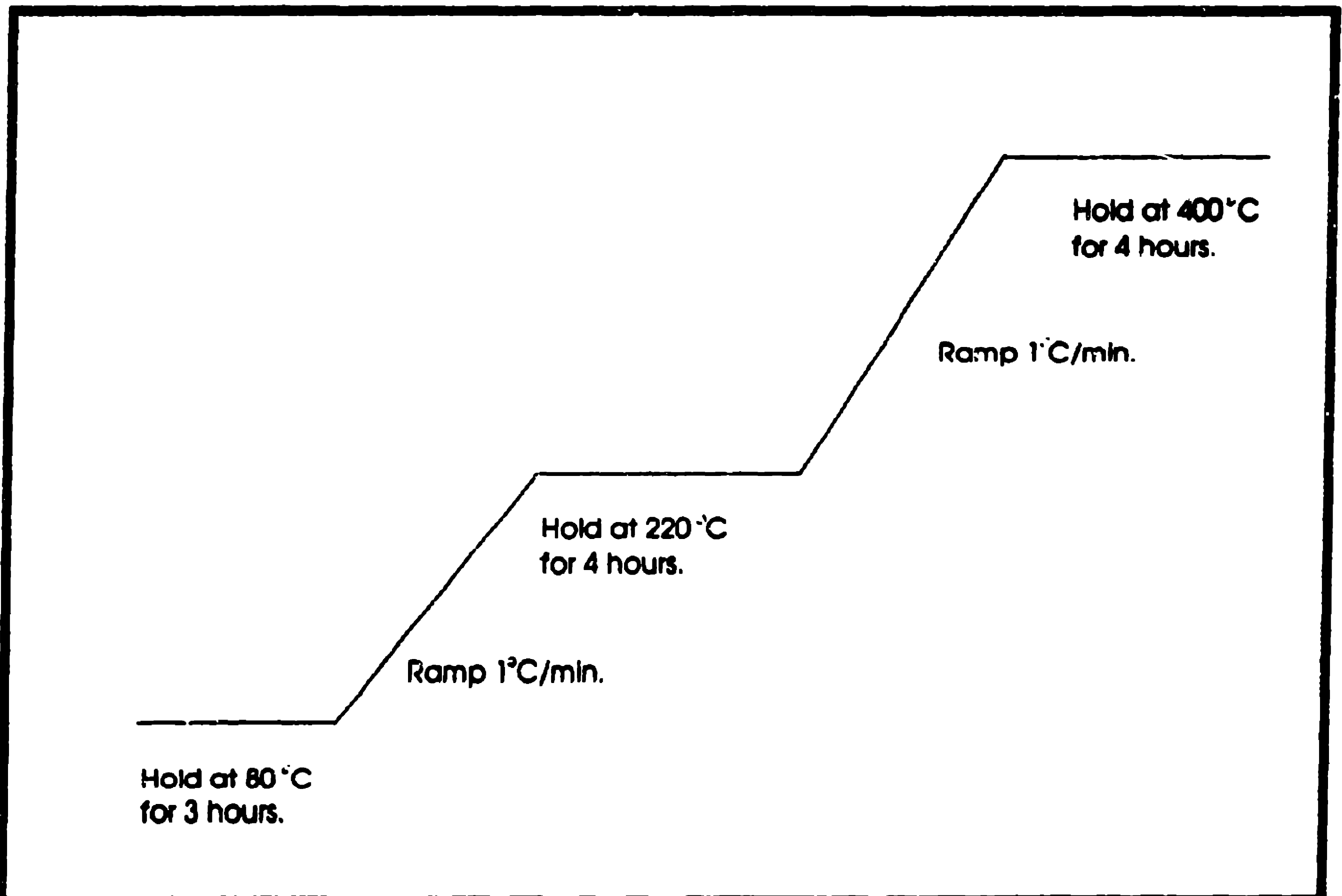

Figure 21. Silver paste curing schedule.

rate and held for an additional 4 hours. Thus, the thermal decomposition of the organic binder from the silver paste occurred outside of the vacuum chamber.

The metal initially chosen for the mounting block was copper for its excellent thermal conductivity, but the copper oxidized during the silver paste curing procedure leaving a layer of loose copper oxide particles on the surface of the block. Though no copper oxide was detected in the YSZ films, to avoid the risk of contamination, the composition of the blocks was changed to nonmagnetic stainless steel. A control experiment confirmed that (200) biaxially aligned YSZ was deposited using the same set of IAD parameters if either the steel or the copper mounting block was used. The block was attached to a steel holder that contained a Borelectric heater (Union Carbide, Advanced Ceramics, Cleveland, OH) and an Inconel sheathed thermocouple so that the temperature could accurately be controlled. Heater control was provided by an Omega 2010 SSR temperature control (Omega Engineering, Inc., Stamford, CT).

3.3 Materials

YSZ and CeO_2 have the fluorite structure shown in Figure 22 for ZrO_2 where the Y^{3+} cation substitutions and O^{2-} vacancies of YSZ were not included. The figure compares the (001) face of YSZ with the CuO_2 plane in the perovskite structure of BYC. Three YSZ unit cells coincide with 4 BYC unit cells for the $\phi = 0°$ orientation. When the [110] direction of YSZ is colinear with the [100] direction of BYC, the oxygen sublattices have about a 6% mismatch in the $\phi = 45°$ orientation [1]. Thus, the (200) orientation of the cubic phase of the YSZ and CeO_2 films was desired perpendicular to the substrate surface for the least amount of lattice mismatch. The 8Y Zirconia (Tosoh Corp., Tokyo, Japan) YSZ evaporation source material contained 8 mol % Y_2O_3 as the stabilizer. Figure 23 shows that YSZ films containing such a high percentage of yttria are cubic even at equilibrium [50]. The CeO_2 source material had a

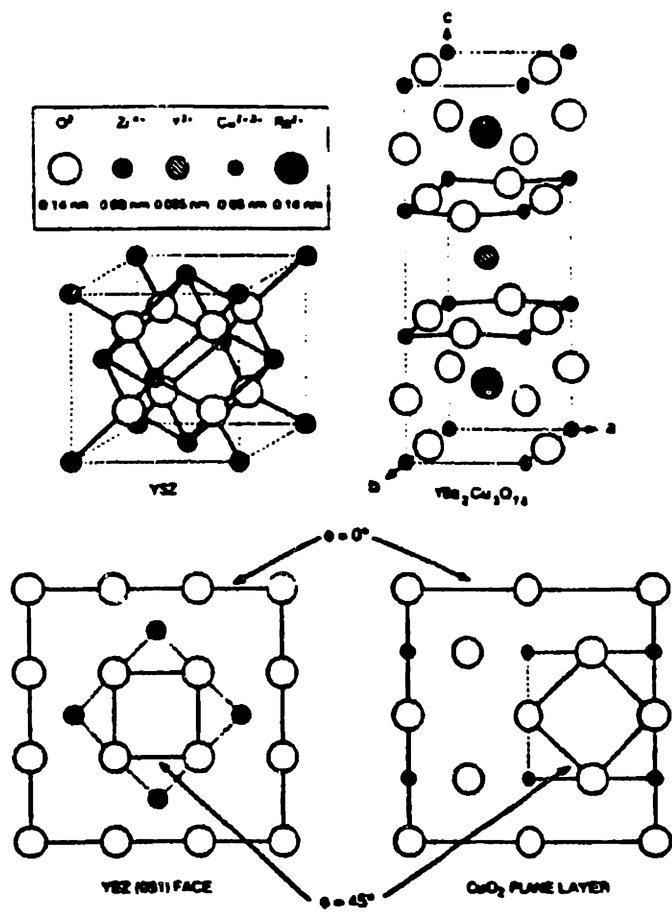

Figure 22. Crystal structures of YSZ, BYC, and {001} plan views of each structure [1].

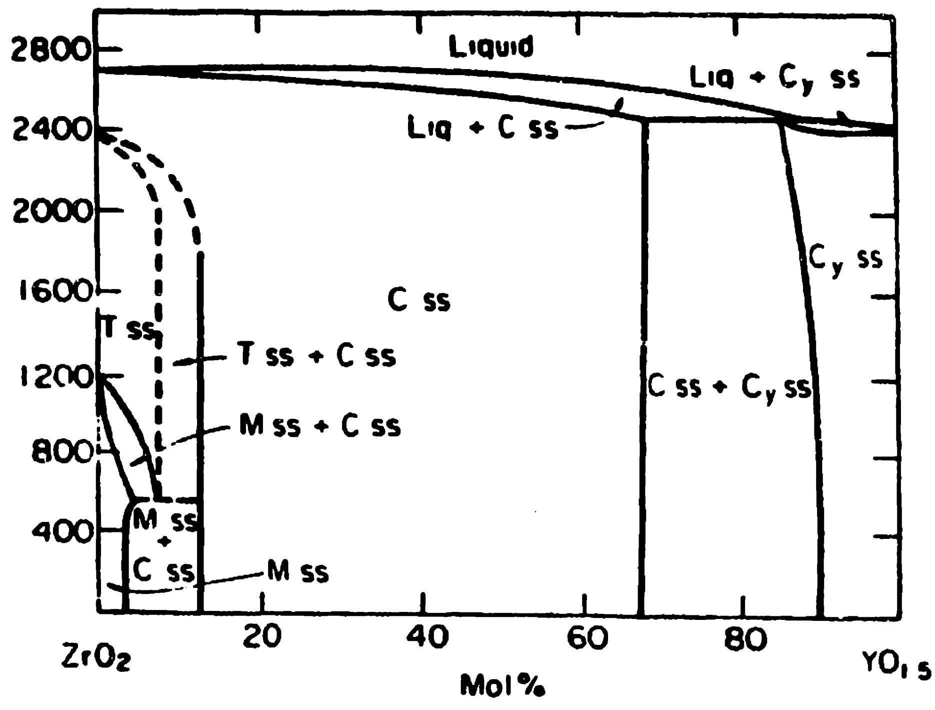

Figure 23. Binary phase diagram of ZrO_2 and $YO_{1.5}$ [50].

purity of 99.9% (Alfa Products, Beverly, MA). The raw powder of both source materials was pressed both uniaxially and isostatically, fired to 1300 °C, and crushed with mortar and pestle into ~3 mm sized pieces. The pieces of source material were placed in the electron gun crucible and then heated gradually by the e-beam under high vacuum conditions. The e-beam power was increased to a specified level and equilibrated before the shutter was removed to start deposition.

Glass substrates consisted of 0.25 inch square, 0.06 inch thick, flat specimens of type 7740 Pyrex (Corning Glass Co., Corning, NY) and soda lime glass. The soda lime glass was included in the study to prevent the cracking of the YSZ film. The coeficient of thermal expansion (CTE) of soda lime glass, 9.0×10^{-6} cm/cm/°C, is close to the CTE of YSZ at 10.0×10^{-6} cm/cm/°C. The CTE of pyrex, however, is 3.25×10^{-6} cm/cm/°C which differs enough from the CTE of YSZ to cause the YSZ films to crack as they cooled after deposition.

3.4 Experimental Parameters

The gas for the ion source was a mixture of argon with 8% oxygen, and pure argon was used for the PBN. Introduction of these gases increased the chamber pressure to 2×10^{-4} Torr which was maintained throughout deposition. Specimens were preheated to 600° C for YSZ deposition and to 400 °C for ceria. The substrates were etched with the ion beam for 10 minutes prior to deposition to insure cleanliness. Films were deposited at rates of either 1.2 Å/s or 2.4 Å/s, and the final films thickness was approximately 1 µm as measured from scanning electron microscope (SEM) micrographs. Film thicknesses were recorded during deposition using a quartz crystal film thickness monitor (Sycon Instruments, Syracuse, NY). The YSZ film was deposited to a thickness of 5000 Å in each experiment as measured by the thickness monitor. The actual thickness of the films is larger than detected during deposition because the monitor is located approxiamately 25 cm above the substrates inside the vacuum chamber. The ion beam energies used

were either 75 eV or 300 eV, and the current density was 18 μA/cm² or 84 μA/cm². The ion beam current density was confirmed independently by placing a Faraday cup at the specimen holder. A 25 V negative bias was applied to the Faraday cup to repel the electrons from the PBN so that the current density of the ions was correctly measured.

3.5 Characterization Techniques

The microstructure of the film was characterized by scanning electron microscope (SEM) (Hitachi S-530) and transmission electron microscopy (TEM) (200 kV, Akashi EM-002B, Japan). X-ray diffraction (XRD) (Rigaku RU-300, Japan) from a copper Kα radiation source was used to study orientation in the films. The degree of orientation normal to the surface of the film was semiquantitatively measured with θ/2θ XRD scans by comparing the ratios of peak intensities for the deposited YSZ and ceria films with the ratios of peak intensities of the randomly oriented powder diffraction patterns for ZrO_2 and CeO_2. The addition of the 8 mol % Y_2O_3 to the ZrO_2 affected the XRD patterns by shifting the experimental peak positions a few tenths of a degree to the left. Electron diffraction patterns of TEM cross-sectional views and planviews were used to cross check XRD data. Rocking curves about the (200) cubic peak indicated the extent of crystalline alignment perpendicular to the surface of the film, and pole figures characterized the in-plane texture of the films.

CHAPTER FOUR
OBSERVATIONS

4.1 YSZ Control Experiments

YSZ films deposited on Pyrex glass at ~200° C without IAD are largely amorphous, as shown by the XRD pattern in Figure 24a. Introduction of the ion beam complicated the deposition process since the substrate temperature was observed to slowly increase with time due to specimen heating from ion bombardment. The substrate temperature would rise to over 200° C during the course of a typical deposition experiment. Deposition experiments, therefore, were performed at high temperature where the substrate temperature could be accurately controlled. Further experiments were conducted at 600° C with constant substrate temperature maintained to within 2 °C throughout deposition.

YSZ films on Pyrex deposited at 600 °C without IAD are crystalline as shown by the XRD pattern in Figure 24b. These films exhibit strong preferential orientation of the grains with the (100) axis perpendicular to the plane of the film. Randomly oriented polycrystalline YSZ exhibits a strong (111) reflection which is hardly evident in this XRD pattern. The (200) reflection, however, is much stronger than the other peaks in Figure 24b. The (111) pole figure for this film, shown in Figure 25, confirms the presence of a strong wire texture. The maximum intensity of the (111) pole appears at an angle approximately 35° with respect to the substrate, but the pole is distributed uniformly in the plane of the film. Thus, only uniaxial orientation is exhibited in YSZ films deposited on Pyrex at 600 °C without IAD.

4.2 (200) Dependence on Ion Bombardment Angle

All YSZ films produced with IAD exhibited predominant (200) orientation with respect to the plane of the film. The absolute intensity of the (200) XRD reflection did,

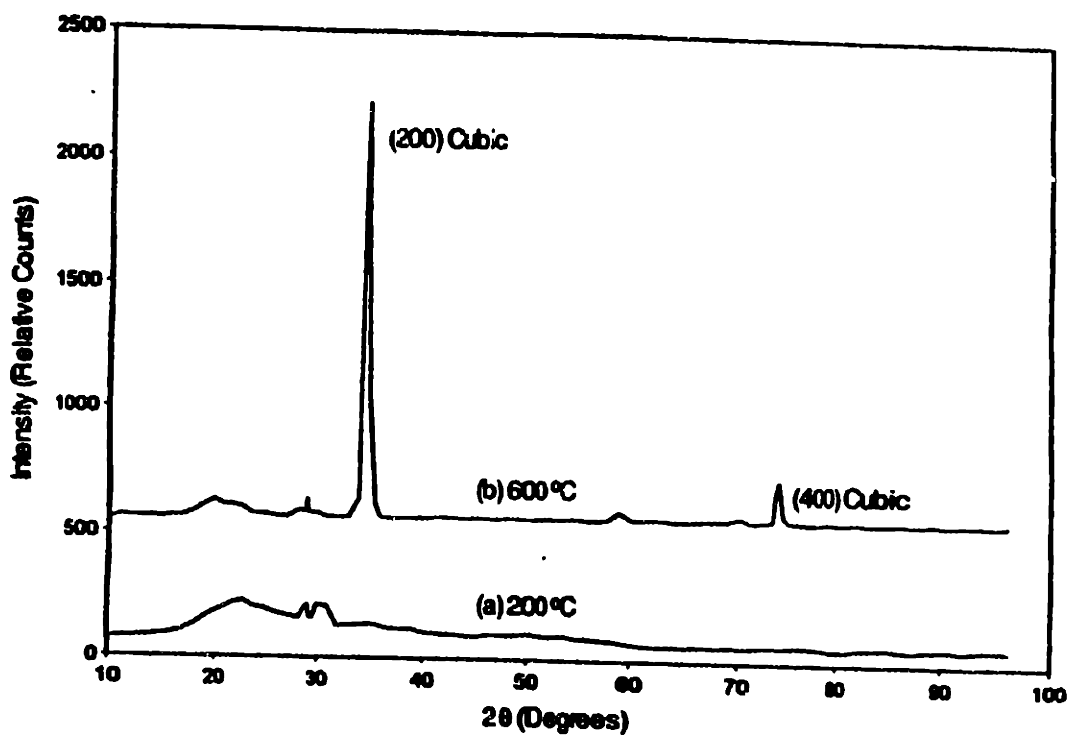

Figure 24. X-ray diffraction patterns of YSZ films on Pyrex deposited at (a) 200 °C and; (b) 600 °C.

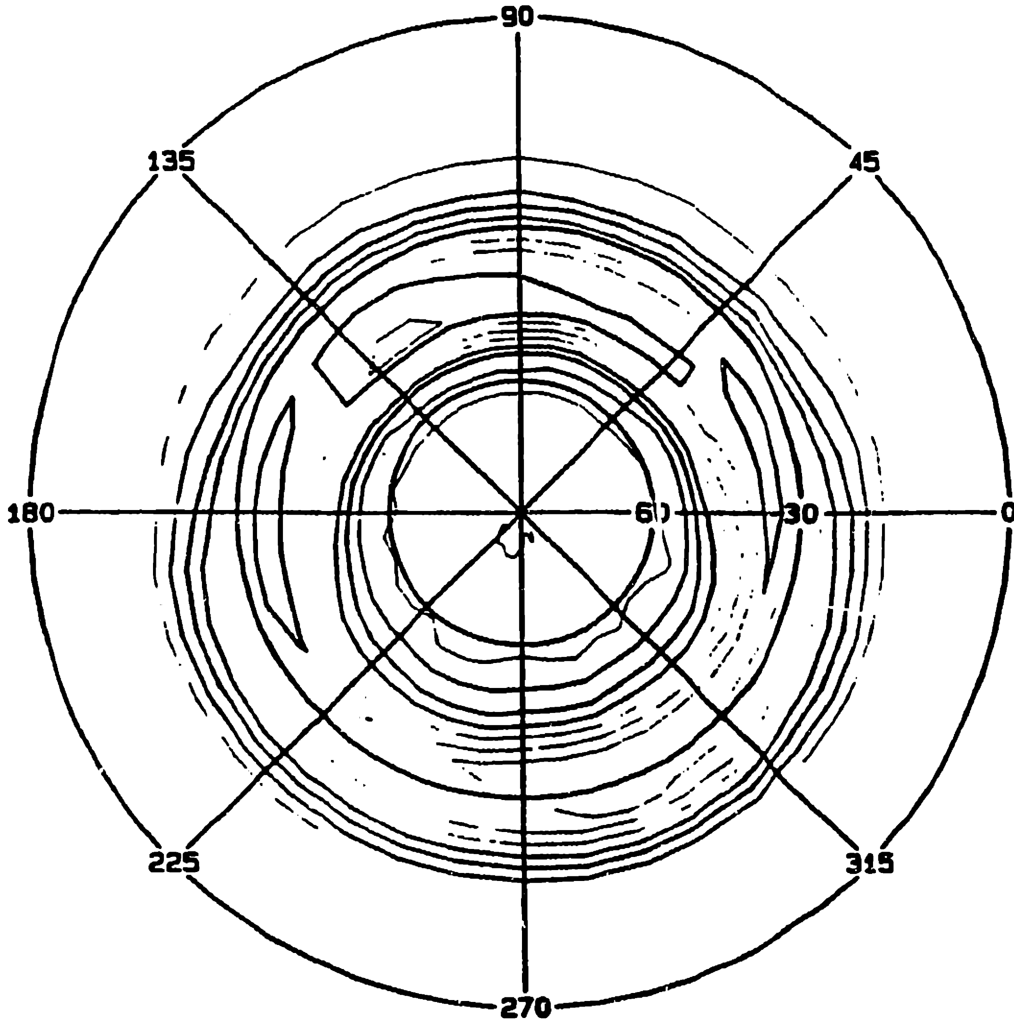

Figure 25. (111) pole figure of YSZ film on Pyrex deposited without IAD.

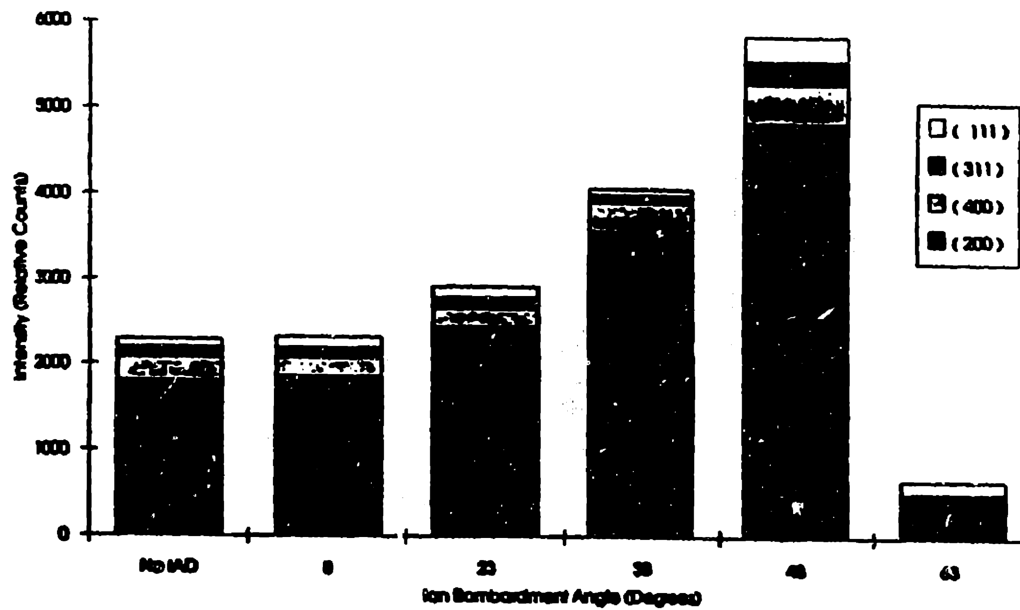

Figure 26. XRD peak intensity versus ion bombardment angle for YSZ film on Pyrex.

however, vary with bombardment angle. Figure 26 depicts the variation in XRD reflection intensity as a function of bombardment angle for samples prepared with IAD. The deposition rate for this series was 2.4 Å/s, the beam current density was 18 $\mu A/cm^2$, and the beam energy was 75 eV. The XRD reflection intensities for a specimen prepared without IAD also are included for comparison. The relative intensities of the (200), (111), (311) and (400) reflections are compared within each bar. Note that the (200) reflection intensity rises to a maximum near 48°. The specimen prepared with IAD at 8° has reflection intensities similar to those produced without IAD. The sample prepared with IAD at 63° has preferred (311) orientation with respect to the substrate. Perfect (100) texture is not observed even at 48°, but the increased (200) reflection intensity indicates substantial improvement in orientation with respect to the plane of the film.

4.3 Dependence of Texture on IAD Parameters

Table 1 summarizes the conditions studied and pole figure results for films deposited using IAD. Four series of films were deposited with differing bombardment angles, deposition rate, ion current density, and beam energy. Figures 27a and 27b show the (111) and (220) pole figures, respectively, for a series 2 film with $\theta = 38°$. The direction marked 0° on the outer edge of each figure is the projected direction of the ion beam in the plane of the film. Restricted wire texture is apparent as the pole figures are not cylindrically symmetric. Four intensity maxima are clearly evident in the azimuthal direction. Figures 27a and 27b are consistent with the cubic symmetry of the YSZ structure since projections of (111) and (220) poles onto the plane of the figure should differ by a rotation of 45°. Thus, the figures show that biaxial alignment occurs such that the direction of the (220) pole corresponds to the direction of the ion beam (Figure 28). The same orientation with respect to the ion beam was exhibited for all bombardment angles in series 2 except for 8°. The pole figure indicates that at 8° a

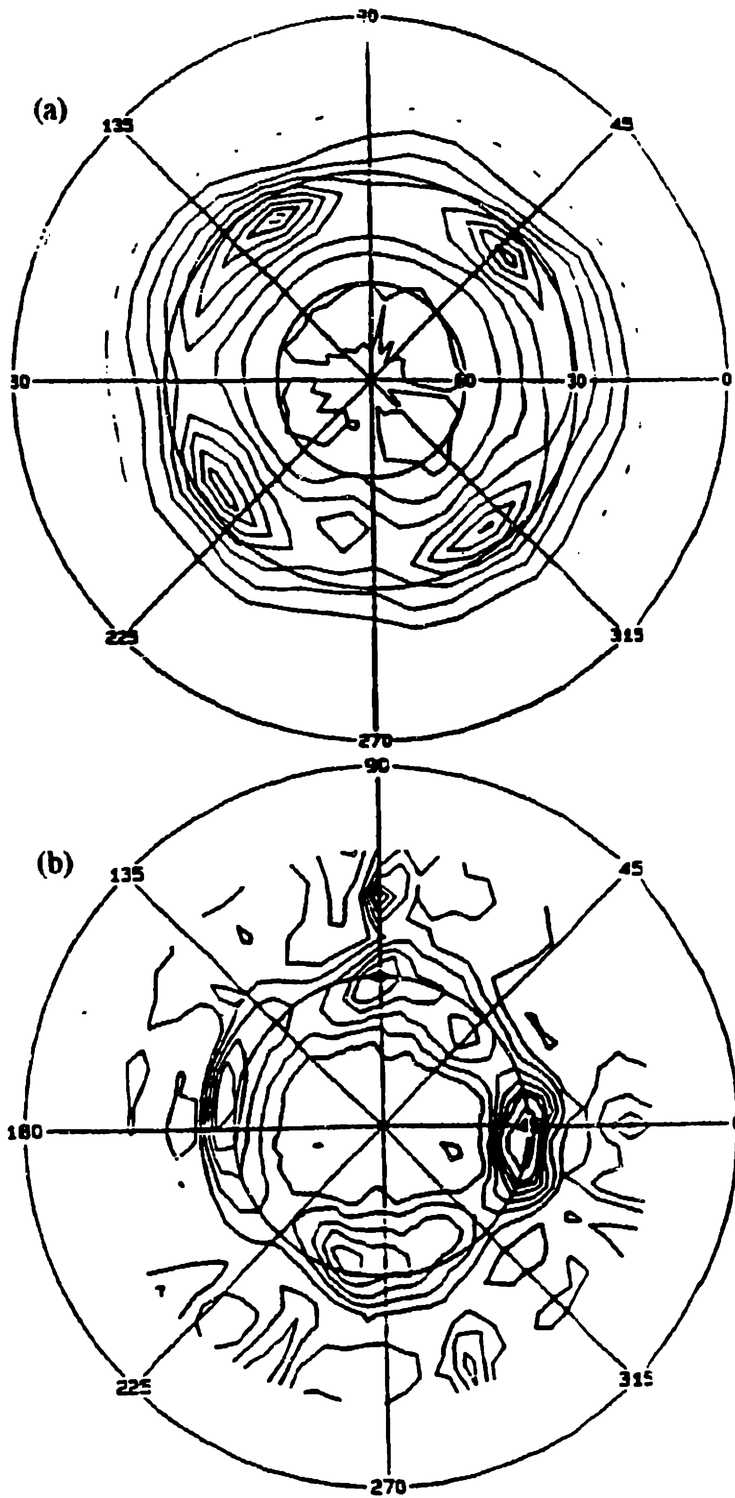

Figure 27. YSZ film on Pyrex: (a) (111) pole figure; (b) (220) pole figure.

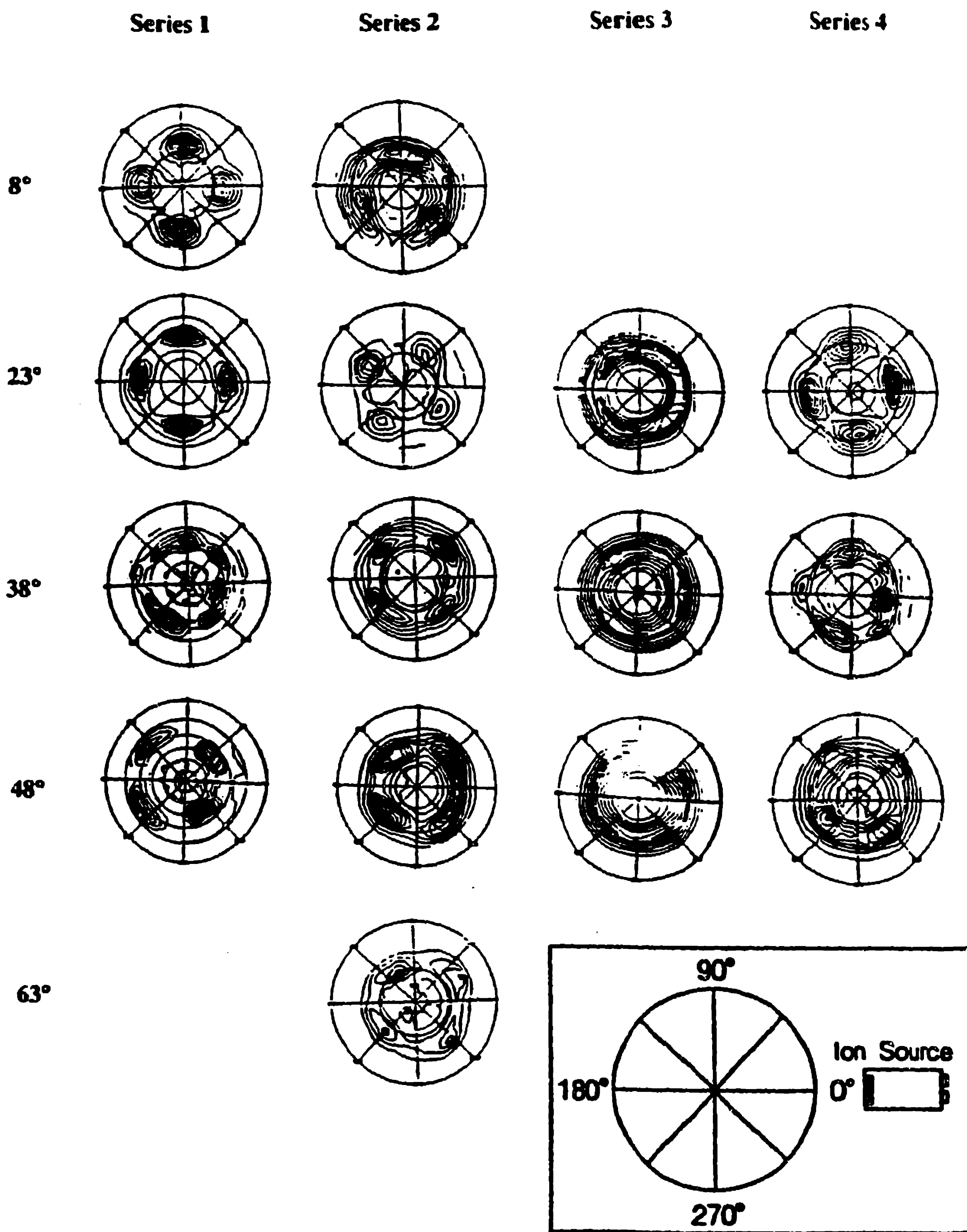

Figure 28. (111) pole figures of YSZ films grown on Pyrex with IAD.

mixture of orientations are present. Contributions of both (111) and (220) orientations in the direction of the ion beam are observed.

Table 1: Biaxially Aligned Plane Parallel to Ion Source				
Series	1	2	3	4
Deposition Rate (Å/s)	1.2	2.4	2.4	2.4
Current Density ($\mu A/cm^2$)	18	18	18	84
Beam Energy (eV)	75	75	300	300
Ion/Atom Ratio	0.11	0.05	0.05	0.25
Bombardment Angle (Degrees)	Orientation			
8	(111)	mixed		
23	(111)	(220)	(220)†	(111)
38	mixed*	(220)*	(220)*†	mixed*
48	(220)*	(220)	(220)†	(220)
63		(220)		

mixed - Contributions from both (220) with (111) in the direction of the ion beam.
* Some wire texture due to (111) alignment in direction of ion beam.
† Some wire texture due to random azimuthal orientation.

The orientation of the film texture with respect to the ion beam can be changed by modifying IAD conditions. Table 1 summarizes the observed orientations for all the conditions studied and the pole figures are shown in Figure 28. A "(111)" appears in the table for conditions where the projection of the (111) pole onto the plane of the pole figure lies in the same direction as the projection of the ion beam direction. Similarly, a "(220)" appears in the table when the (111) pole projection is 45° with respect to the projection of the ion beam direction. The table indicates "mixed" if both (111) and (220) contributions were evident in the pole figure.

The influence of ion current density and deposition rate on the orientation of IAD films has not previously been reported. Iijima et al. [12,13] reported that the (111)

orientation was in the dir-·tion of the ion beam for all conditions used in their study. The deposition rate used was 0.5 Å/s with an ion fluence of 220 μA/cm² and a beam energy of 300 eV. Table 1 suggests that the ratio of ion intensity to film deposition rate is an important factor in determining film orientation. The ratio of ion flux to atom flux (r) is only 0.05 for the conditions used in series 2 and 3. Series 1 and 4 have r equal to 0.11 and 0.25, respectively. Iijima et al. [12,13] deposited YSZ films under much higher ion intensity, such that r equalled 3.1. Apparently, greater r favors orientation of the (111) axis of the crystallites toward the ion beam for bombardment angles of 23° or lower.

All films deposited at 38° and the film in series 1 deposited at 48° exhibit an intense single pole parallel to the ion beam associated with wire texture due to (111) alignment in the direction of the ion beam. Both series 1 and 4 show (111) orientations at low angles (<23°), mixed orientations at 38°, and are (220) oriented at 48°. Series 2 and 3 always are (220) oriented, with the exception of the film in series 2 deposited at 8° which has mixed (111) and (220) orientations. From these results, it appears that ion bombardment angle has a pronounced effect on orientation at greater values of r. The effect of different values of r on orientation was not discussed by Iijima et al.

Orientation appears to be independent of ion beam energy in the range of 75 eV to 300 eV. Series 2 and 3 differ only by the energy of the ion beam; the deposition rate and ion current density are 2.4 Å/s and 18 μA/cm^2 respectively. In both series, the orientation of the texture is such that the (220) projection is parallel to the ion beam projection. The wire texture in series 3 reveals that at 300 eV the crystallites become uniaxially aligned in the (200) direction, but less strongly oriented in the plane of the film. Films deposited at an ion impingement angle of 48° exhibit in-plane (220) orientation. The (220) plane makes a 45° angle with the (200) plane, so at 48° the direction of the ion beam lies in the (220) channeling direction.

All films deposited at 38° exhibit some form of wire texture. The (111) plane and the (200) plane are separated by 35.3°. Therefore, when the substrate angle is 38°, the ion beam is almost parallel with the (111) channeling direction. The resulting pole figure exhibits a (111) pole at 0° which is the direction of the ion beam projection on the plane of the film. Series 4 shows that increasing the ion current density to 84 $\mu A/cm^2$ at a beam energy of 300 eV also creates the (111) wire texture at 38°. Similarly, in series 1 the (111) wire texture is created by decreasing the deposition rate from 2.4 Å/s to 1.2 Å/s at ion impingement angles of 38° and 48° when the ion current density is 18 $\mu A/cm^2$ and the beam energy is 75 eV.

The best film deposited at 48°, using series 2 IAD conditions, had a (200) XRD reflection with 9258 counts/s. The rocking curve about the (200) peak for the film had a full width at half maximum (FWHM) of 10.8°. In contrast, the FWHM of the (200) peak is 3° showing the film is predominately epitaxial for YSZ deposited on single crystal $SrTiO_3$ substrates during the same deposition experiments. In addition, rocking curves for some specimens exhibit asymmetry indicating that the (200) plane is tilted in a direction other than perpendicular to the plane of the film and is oriented more toward the ion beam. The irregular shape of a few rocking curves also may indicate that some tetragonal phase is mixed with the cubic phase.

4.4 Microstructural Characterization

Preliminary TEM and electron diffraction plan view and cross-sectional studies were performed on a series 2 specimen having a bombardment angle of 48°. This specimen was chosen because it displays the best biaxial alignment with the highest intensity (200) XRD peak, and the pole figure revealed well localized poles. A TEM micrograph and electron diffraction pattern for the plan view section is shown in Figure 29. The film appears granular, but the wide area electron diffraction pattern for the plan view section indicates strong four-fold symmetry consistent with (200) biaxial alignment. A cross-

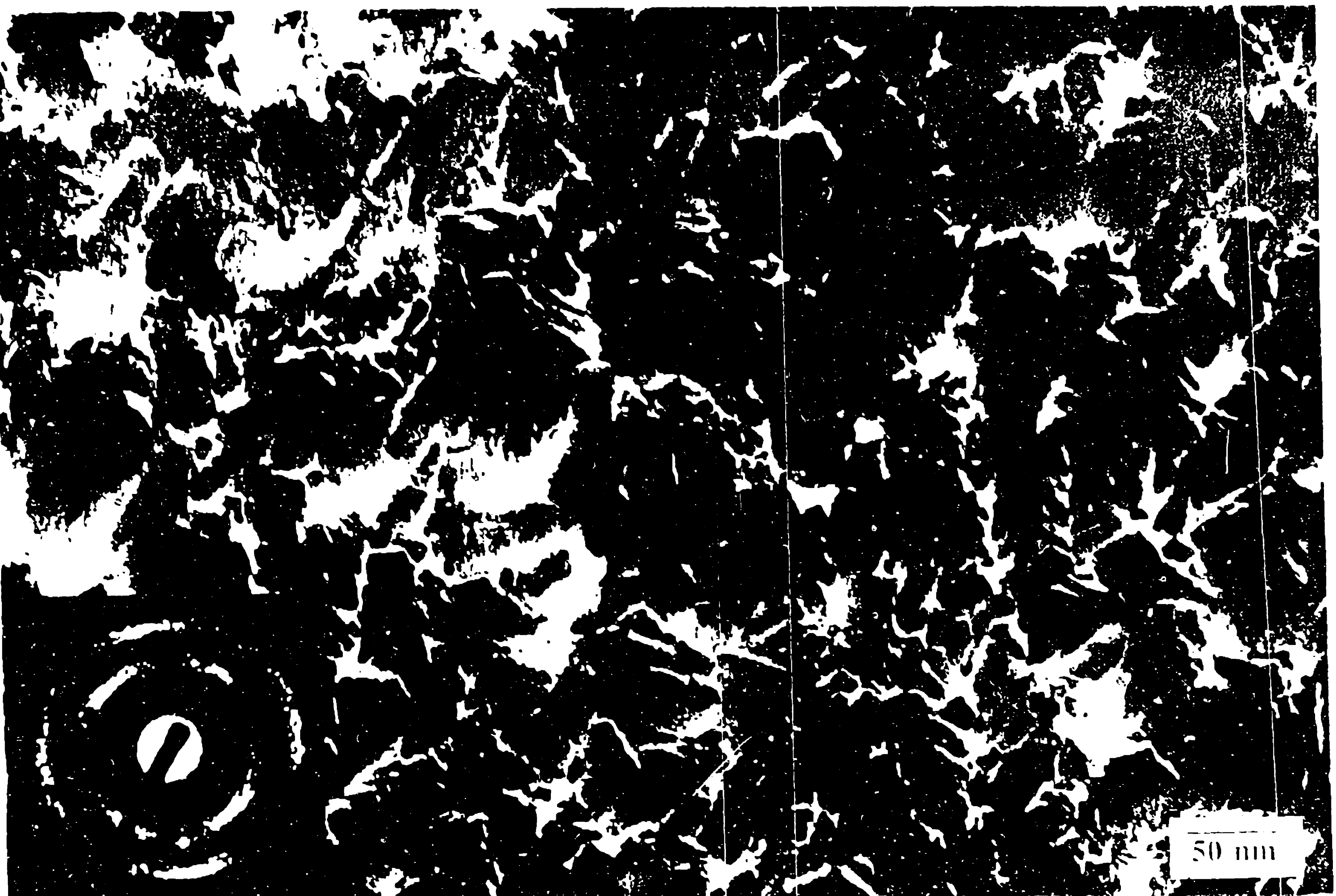

Figure 29 Plan view TEM micrograph and electron diffraction pattern of YSZ film surface

Figure 30. Cross-section TEM micrograph and electron diffraction pattern of YSZ interface.

sectional TEM micrograph and electron diffraction pattern is shown in Figure 30. The columnar structure of the film is apparent. The grain width is approximately 200 Å to 300 Å, but may extend through the thickness of the film. The electron diffraction pattern exhibits uniaxial symmetry consistent with the (100) orientation of the film. The pattern is not consistent, however, with the planview section. Many high order reflections in Figure 30 suggest a wire-type texture perpendicular to the plane of the film. We believe that the short grains near the film/substrate interface contribute to the in-plane misorientation and that the plan view section shown in Figure 29 is mostly composed of long grains which extend though the film.

4.5 Ion Induced Sputtering

The effects of sputtering during film deposition are observed by comparing the film thickness produced with and without IAD. The film thickness was approximately 1 micron for all series of IAD experiments. The thickness, however, was nearly 1.4 microns for a film deposited without IAD but having the same deposition conditions. Films prepared both with and without IAD possess a columnar structure though the density of the columnar structure changes significantly for different IAD conditions. The highest density film was deposited at 38° where the ion beam lies in the (111) channeling direction. A typical SEM plan view and cross section of a biaxially aligned YSZ film is shown in Figure 31. The columnar structure appears to contain residual porosity. Martin *et al.* [32] reported a lower water absorption rate for similarly prepared YSZ films upon removing the specimens from vacuum, which is consistent with a denser microstructure. Film density changes due to ion bombardment make it difficult to quantitatively assess the amount of sputtering.

The influence of sputtering on biaxial alignment was addressed in an experiment where 600 Å of YSZ film was deposited at a rate of 2.4 Å/s with the ion beam off. The shutter over the evaporation source was then closed, and the ion beam turned on so that

(a)

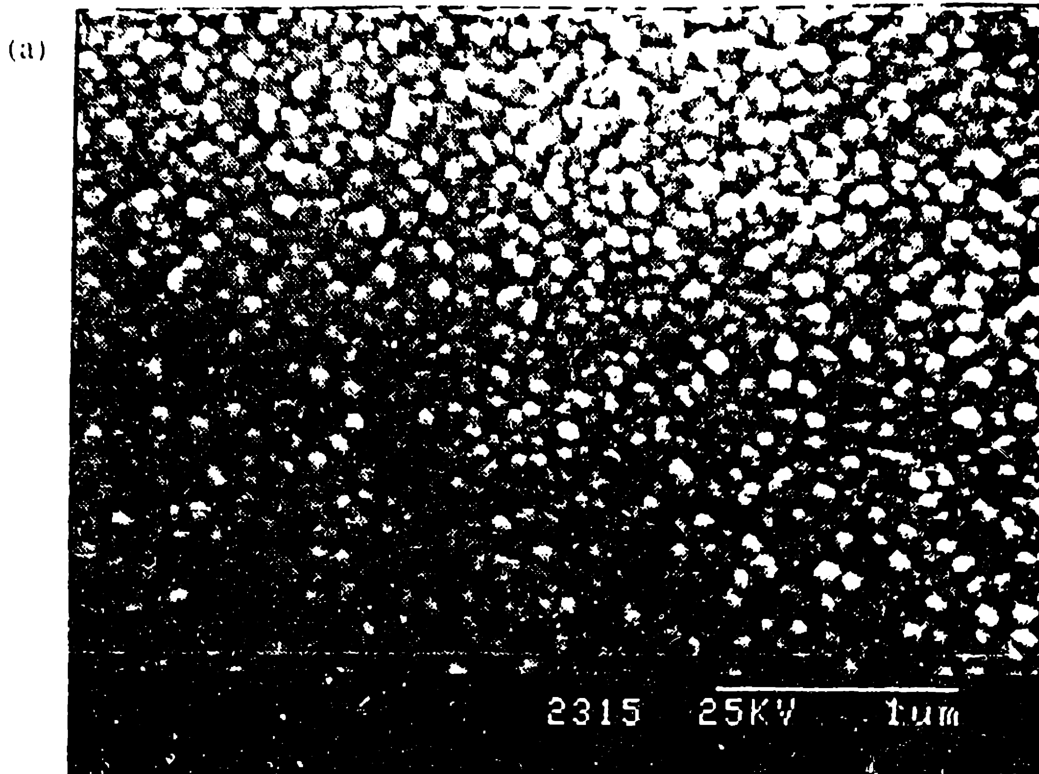

(b)

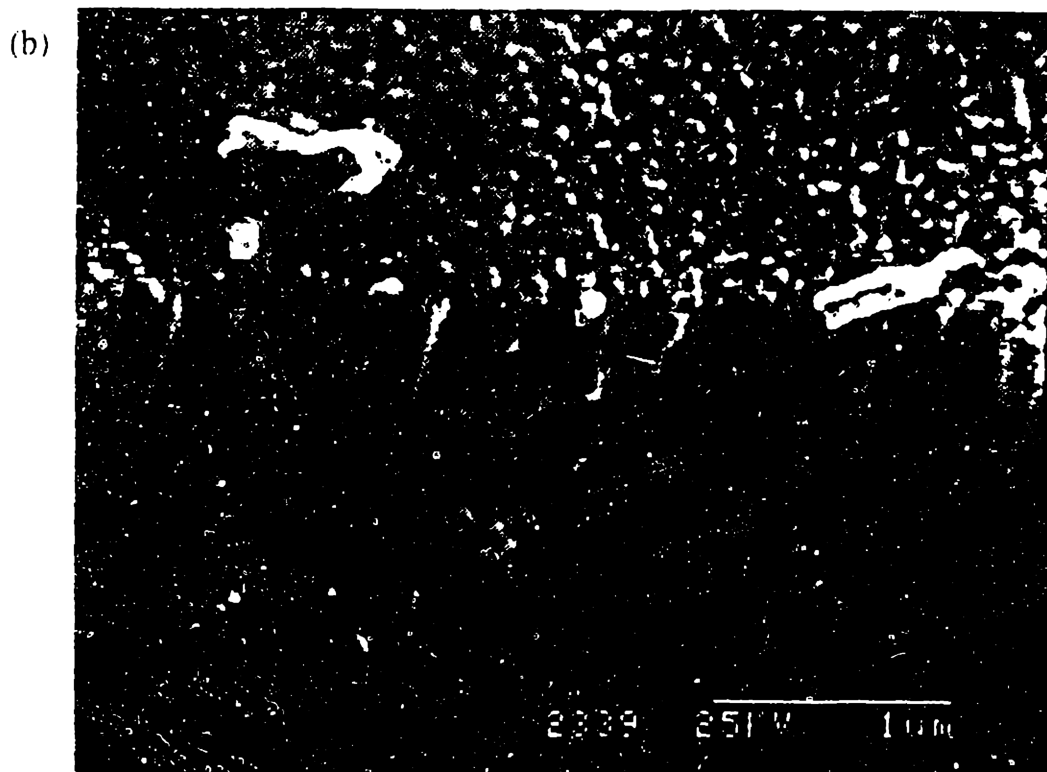

Figure 31. SEM (a) planview and (b) cross section of YSZ film.

the existing YSZ thin layer of film was bombarded with ions for ten minutes. The experimental conditions used were an angle of 48°, an ion current density of 18 $\mu A/cm^2$, and a beam energy of 75 eV. The ion beam then was turned off, and the shutter over the evaporation source was removed so that deposition continued until the film reached a thickness of 1 micron. The resulting pole figure (Figure 32) exhibits some wire texture due to random in-plane alignment of the (200) oriented YSZ film, but superimposed on this are four poles associated with (220) biaxial alignment. These poles are not as intense or as well defined as those observed in the best films produced here.

The influence of IAD during the early stages of growth was examined by turning off the ion beam after a thin layer of YSZ was deposited. A 600 Å film was deposited under the same conditions used for a series 2 film with a 48° ion bombardment angle. The ion beam then was turned off, but deposition continued to a film thickness of 1 micron. The pole figure for the resulting film exhibits strong biaxial alignment, as shown in Figure 33. The experiment confirms that IAD has a strong influence on film microstructure during the initial stages of growth.

4.6 Characteristics of Ceria Films

Biaxially aligned CeO_2 films on Pyrex were deposited at $\theta = 45°$ with an ion current density of 18 $\mu A/cm^2$, a beam energy of 75 eV, and a deposition rate of 2.4 Å/s, but at a lower temperature than used for YSZ films because at 600 °C the ceria was largely (311) oriented as indicated in Figure 34. SEM micrographs of this film in Figure 35 show narrow columns with pointed, faceted tops separated by distinct grain boundaries. Ceria films deposited at 400 °C with the same ion parameters were (200) oriented as shown in Figure 36. The rocking curve of the film, given in Figure 37, had a FWHM of 7.6°, which is 3.2 degrees narrower than the FWHM of the best YSZ film. The (111) pole figure of this film, shown in Figure 38, indicates strong biaxial alignment with the normal to the (220) plane in the direction of the ion beam as it was in the corresponding

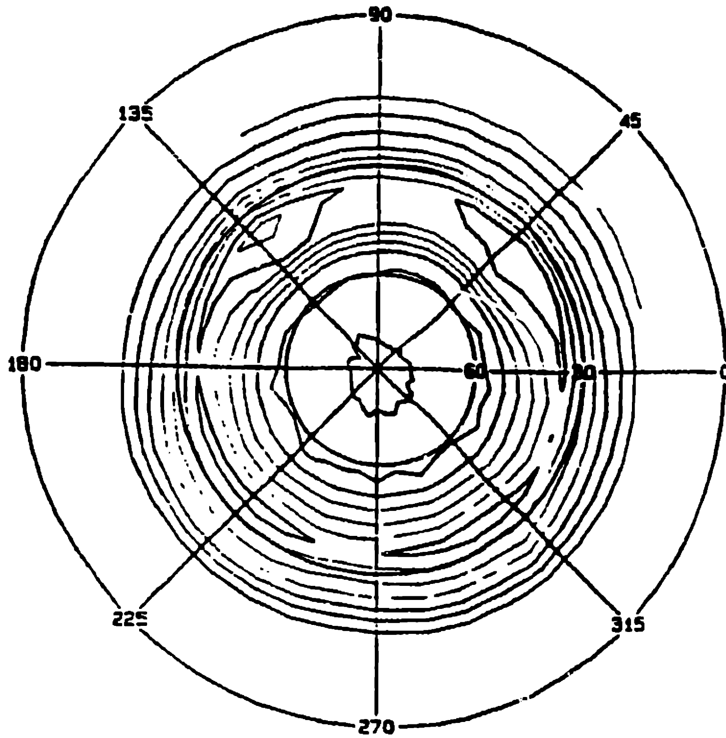

Figure 32. (111) pole figure of specimen prepared by depositing 300 Å without IAD, then turning on the ion beam for 10 min. without YSZ deposition, and then turning the ion beam off until final thickness was reached.

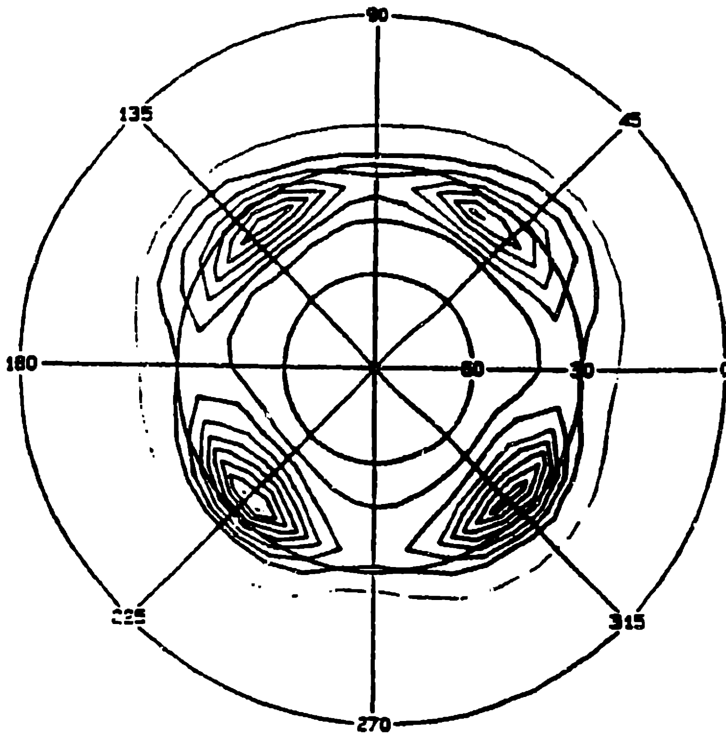

Figure 33. (111) pole figure of biaxially aligned YSZ film grown with only initial use of IAD.

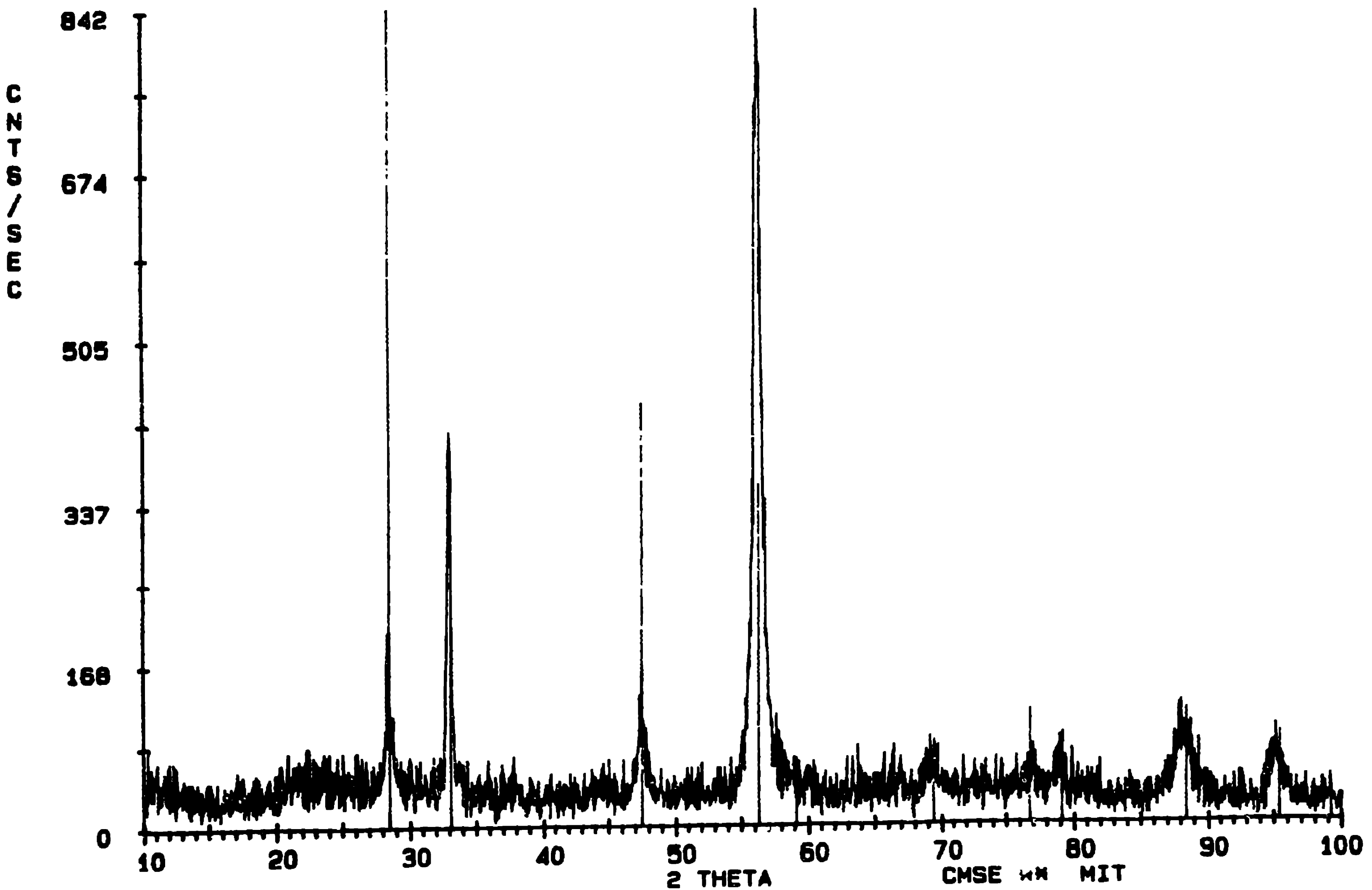

Figure 34. XRD pattern of ceria film grown on Pyrex at 600 °C using IAD.

Figure 35. SEM (a) plan view and; (b) cross-section view of (111) ceria film grown on Pyrex using IAD at 600 °C.

(a)

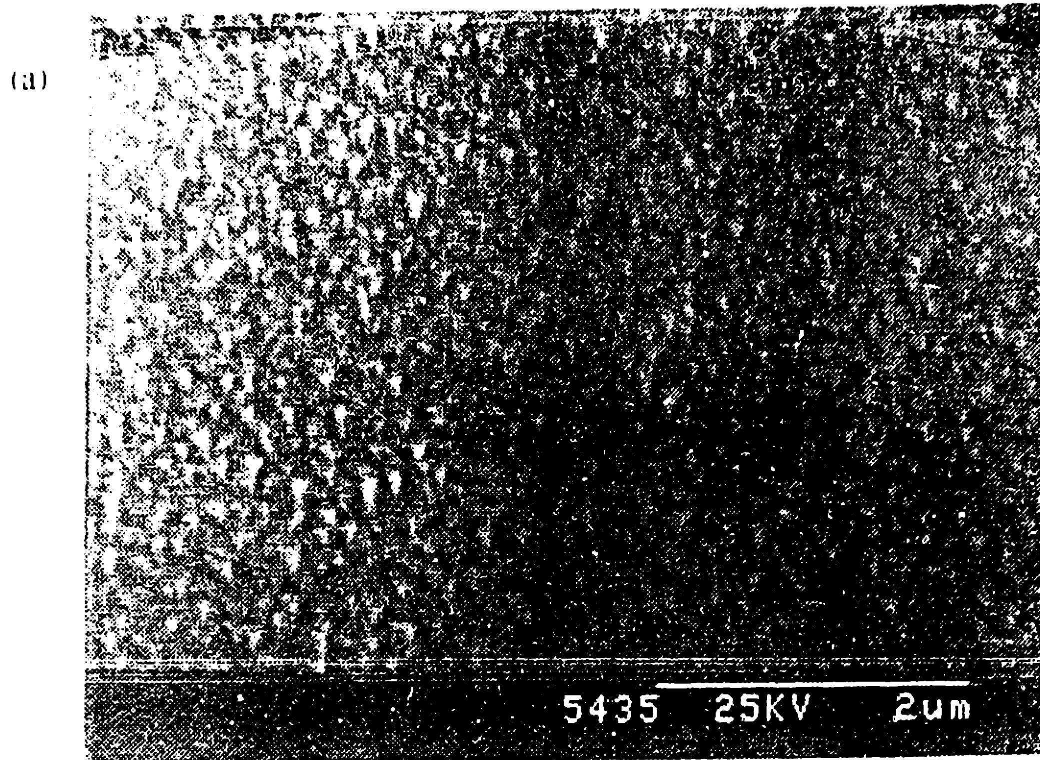

(b)

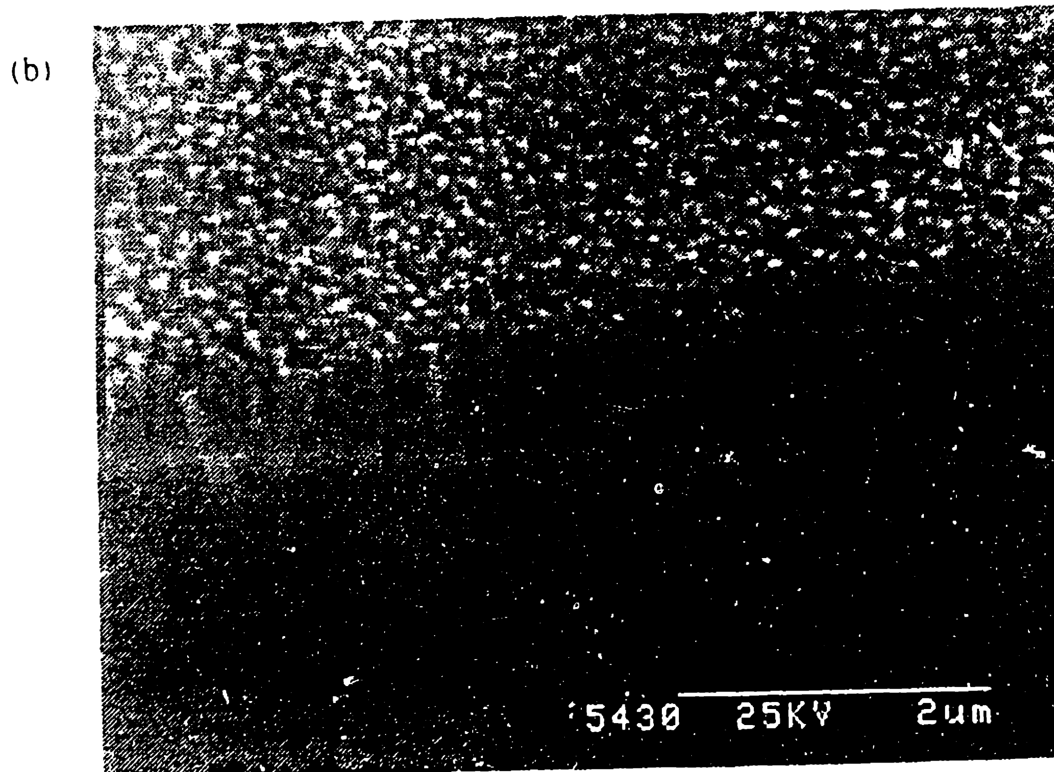

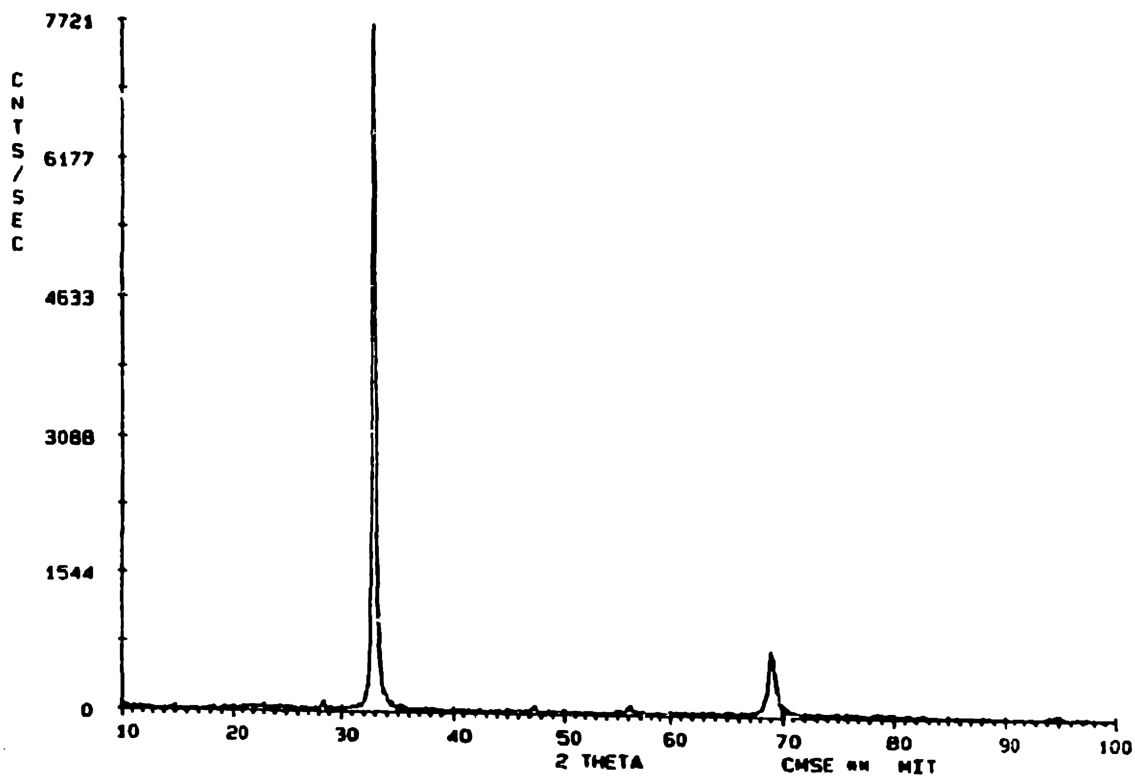

Figure 36. XRD pattern of (200) oriented ceria film grown using IAD at $\theta = 45°$.

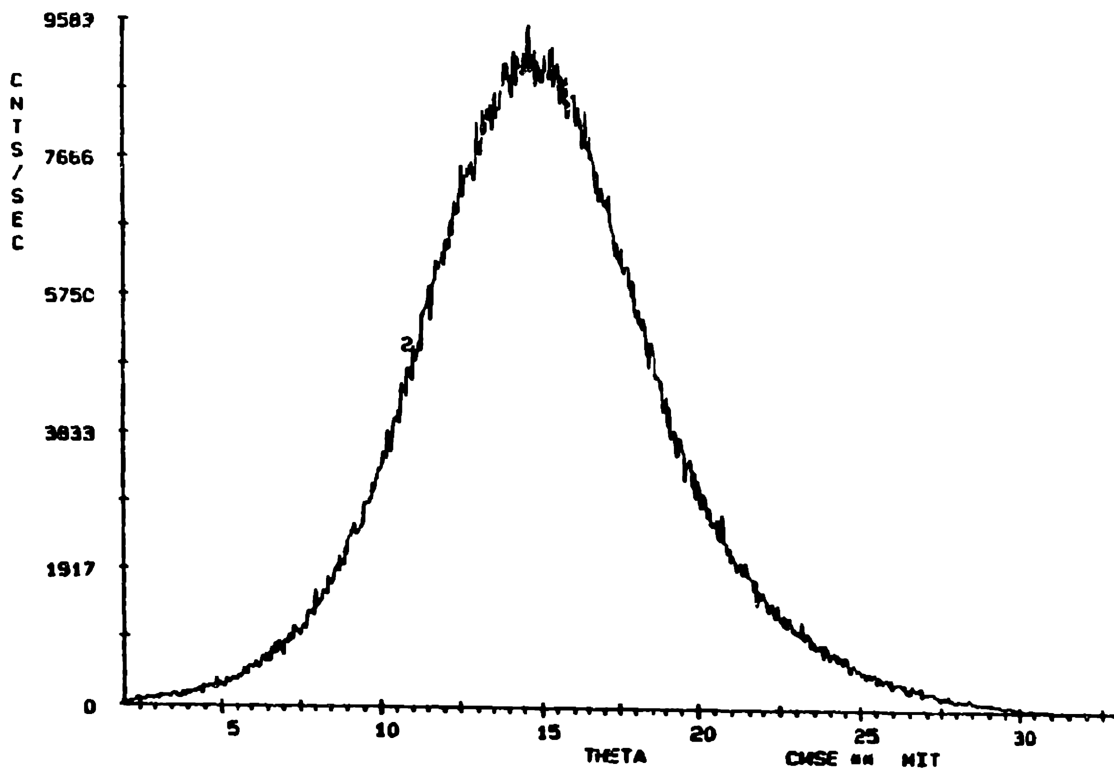

Figure 37. Rocking curve of (200) oriented ceria film grown using IAD at $\theta = 45°$.

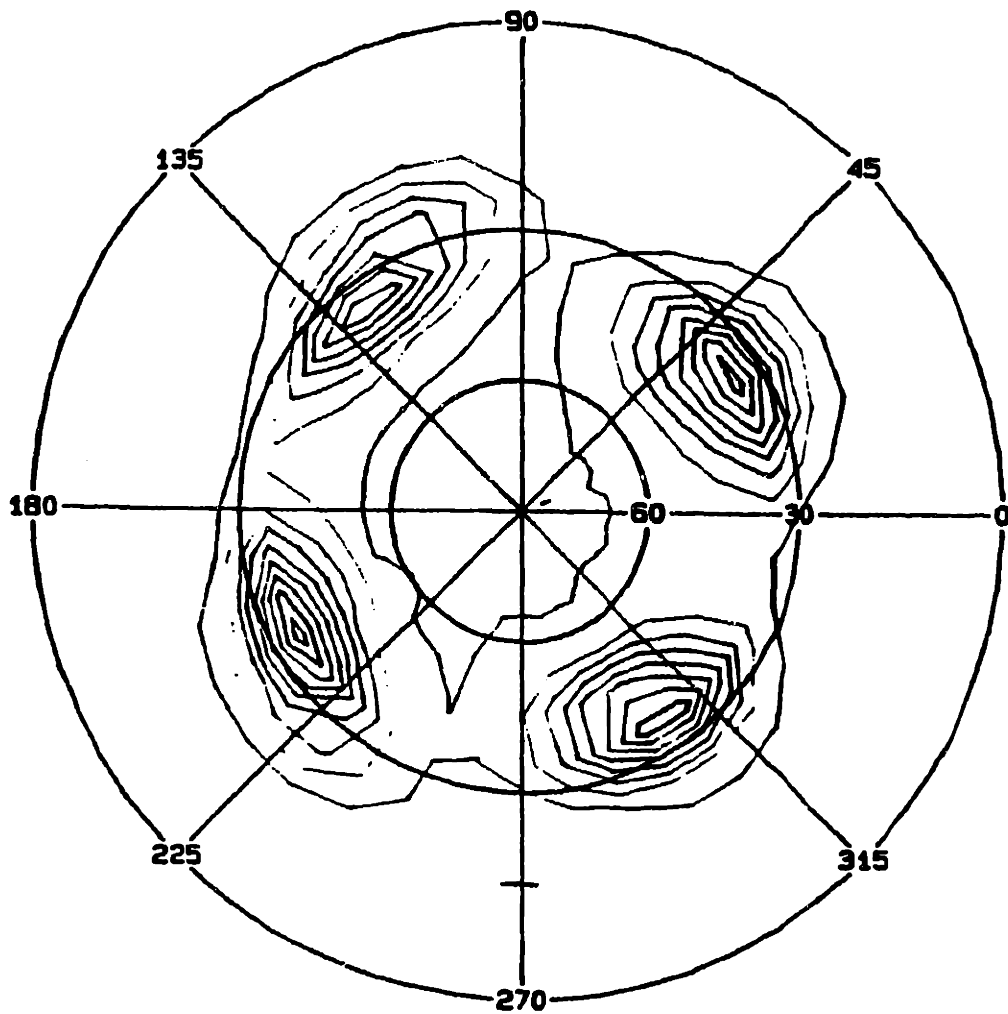

Figure 38. (111) pole figure of ceria film on Pyrex grown using IAD at $\theta = 45°$.

YSZ film. Figure 39 shows the SEM micrograph of this ceria film and reveals a cross-hatched microstructure different from the surface of the YSZ film. The cross-hatched microstructure have may resulted from the combination of biaxial alignment and faster growth along one crystallographic axis.

The resulting microstructure changed, however, when ceria was deposited at the same conditions on soda lime (plate) glass. The XRD pattern in Figure 40 for ceria on plate glass shows (111) orientation. SEM micrographs in Figure 41 reveal elongated faceted grains coming to a point at the surface. The effect of the angle of ion incidence on microstructure was investigated by changing θ to 35° while all other ion parameters remained the same and depositing ceria on Pyrex. The XRD scan for this film in Figure 42 indicates (200) oriented film. The surface microstructure appears different, however, from ceria deposited at $\theta = 45°$; instead of a cross-hatched appearance, the columns have more rounded tops, as shown in Figure 43. At 35°, the cylindrical grains indicate the in-plane crystallographic directions have similar growth rates. A control experiment in which ceria was deposited without the ion beam at 400 °C produced (200) oriented film as did the control experiment for YSZ at 600 °C.

Figure 39. SEM (a) plan view and: (b) cross-section view of (200) ceria film grown on Pyrex using IAD at θ = 45°.

(a)

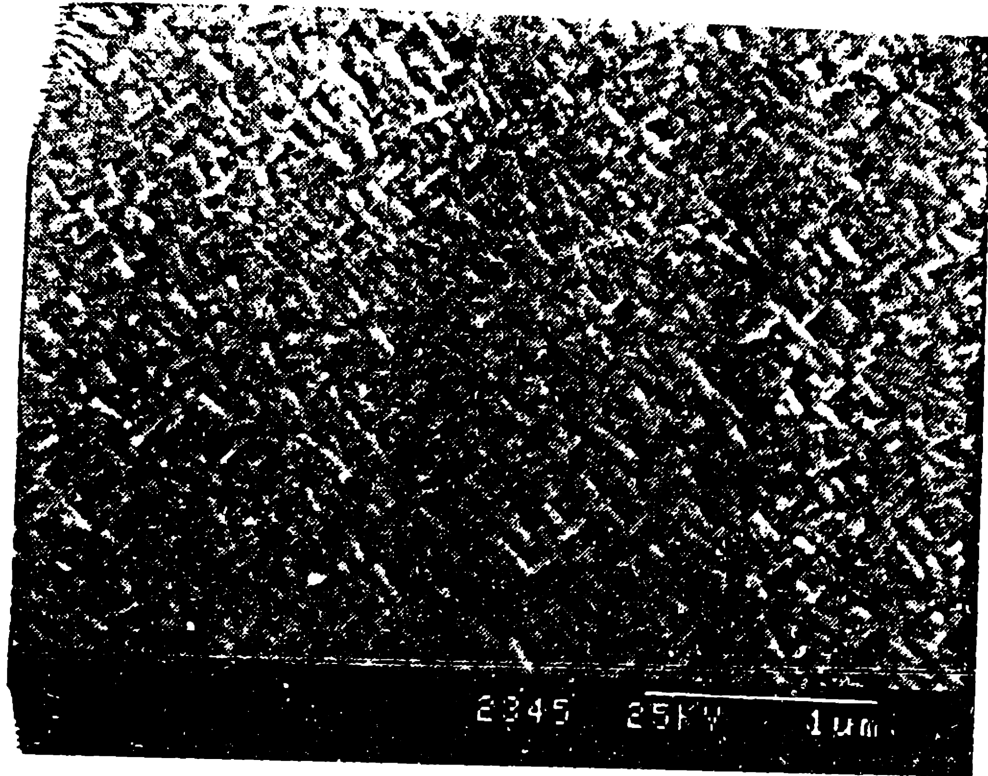

(b)

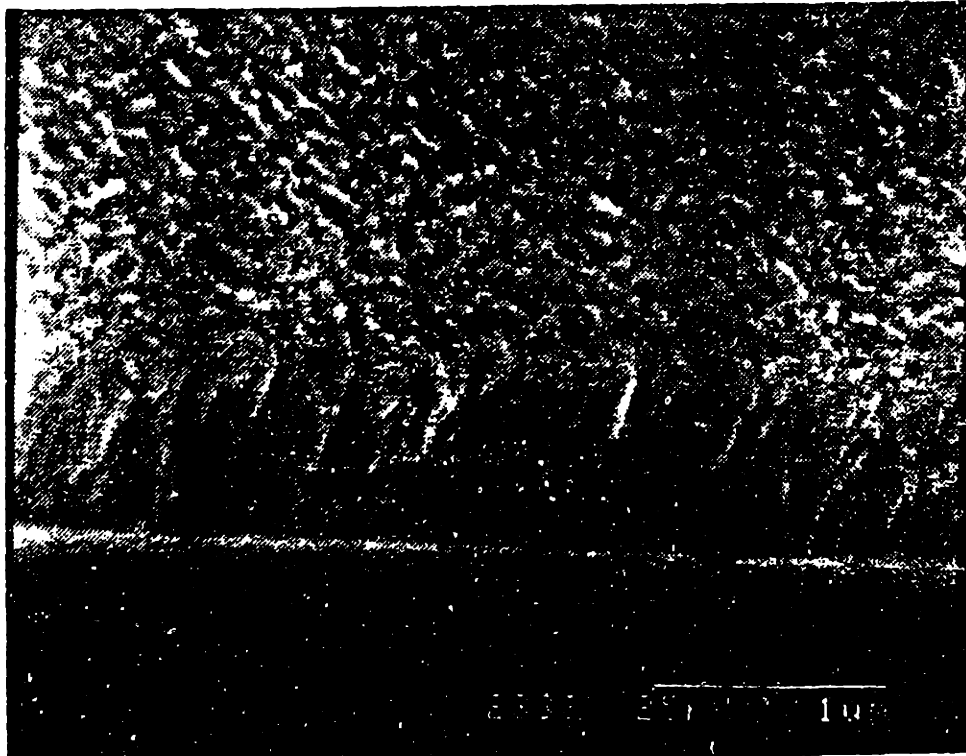

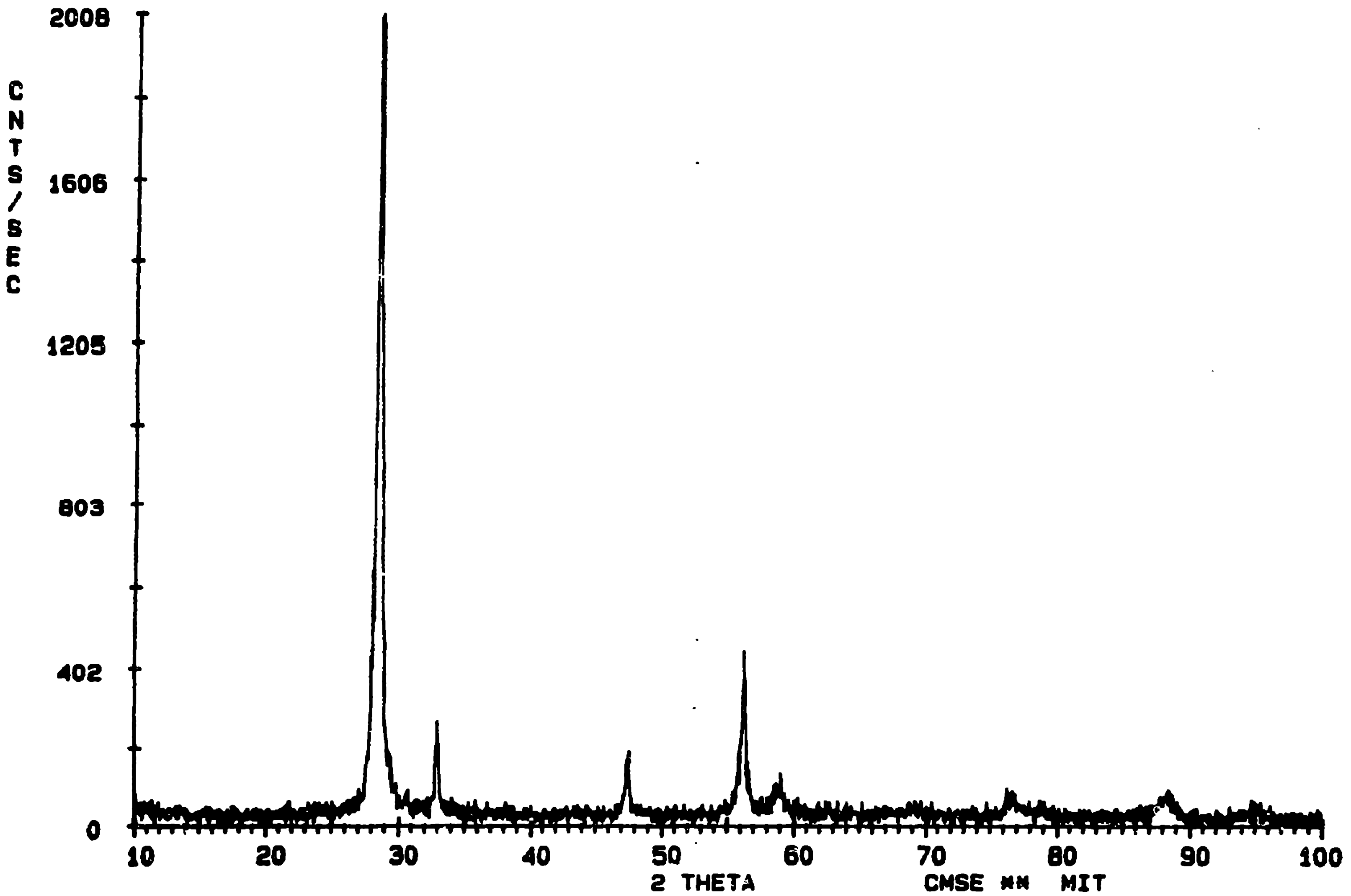

Figure 40. XRD pattern of (111) oriented ceria film grown on soda lime glass using IAD.

Figure 41. SEM (a) plan view and: (b) cross-section view of (111) ceria film on soda lime glass.

(a)

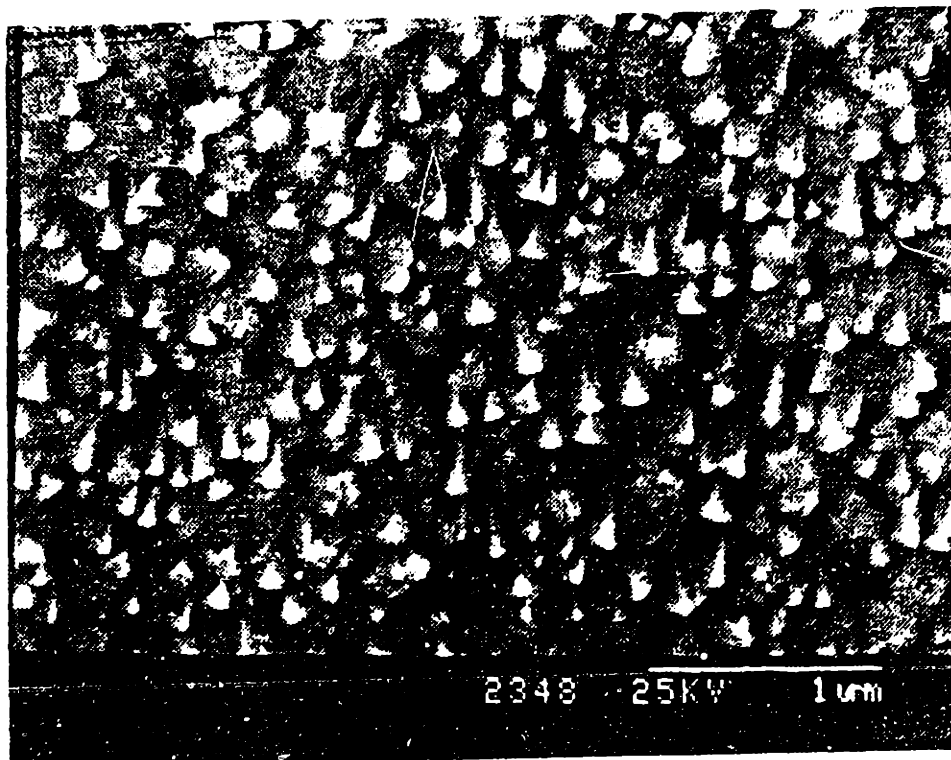

(b)

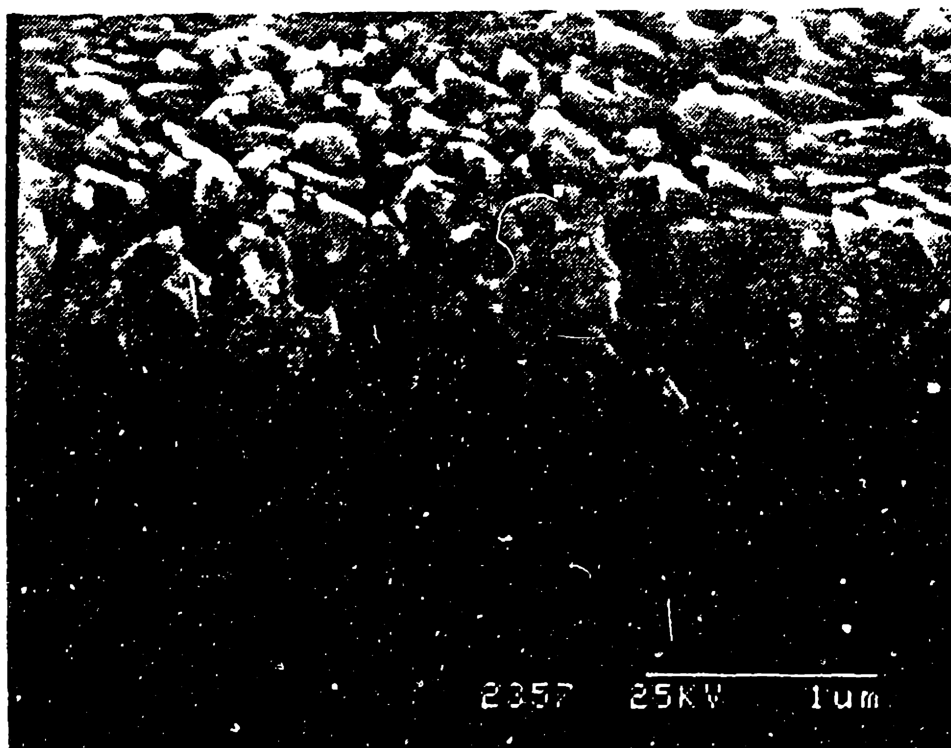

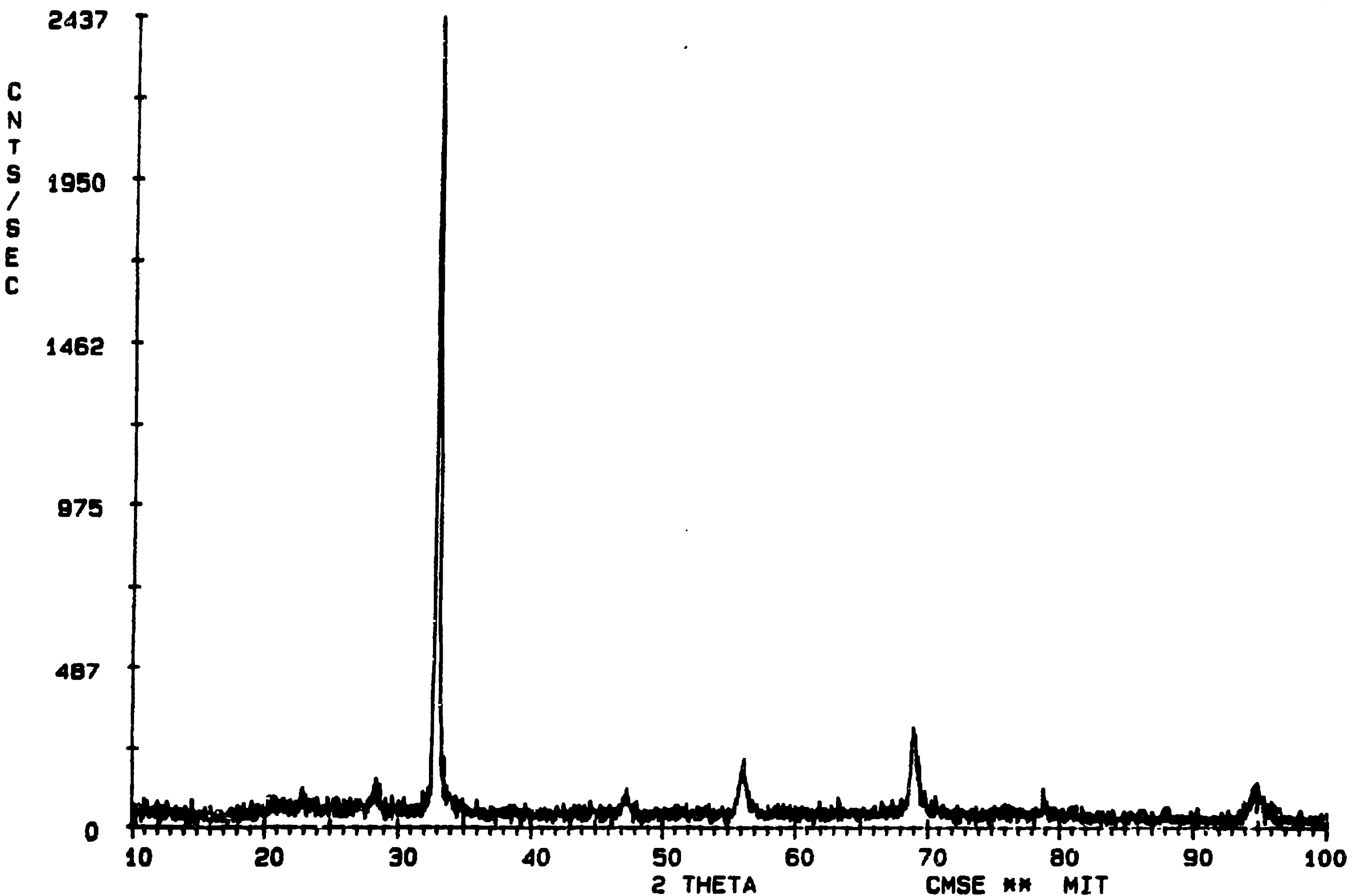

Figure 42. XRD pattern of (200) oriented ceria film grown using IAD at $\theta = 35°$.

Figure 43. SEM (a) plan view and: (b) cross-section view of (200) ceria film grown on Pyrex using IAD at $\theta = 35°$.

(a)

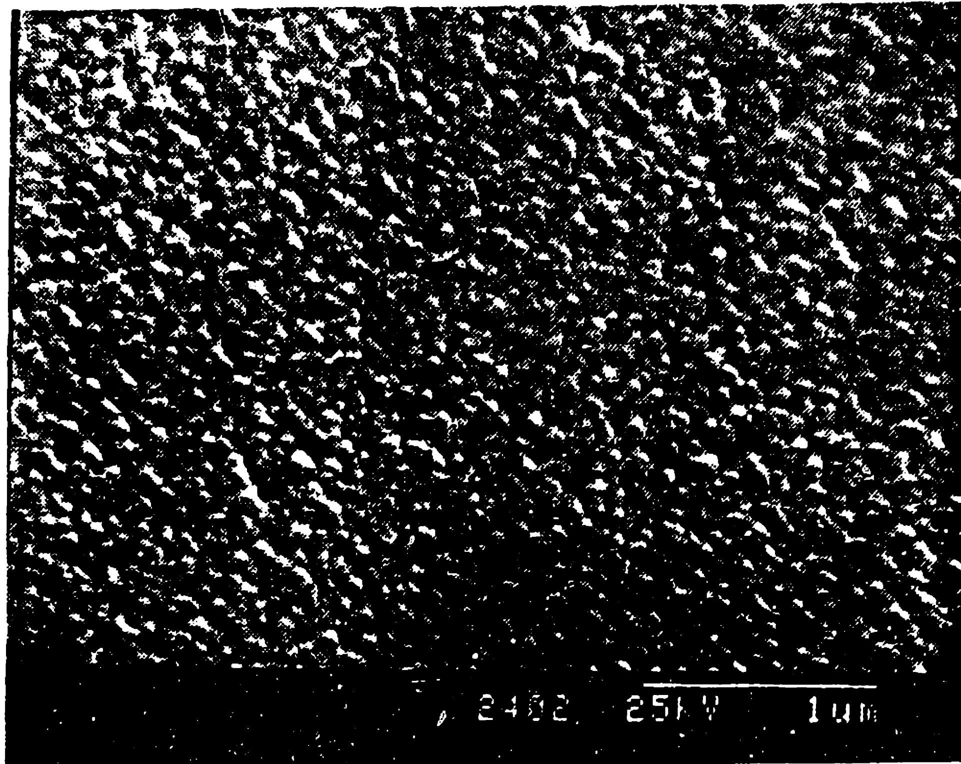

(b)

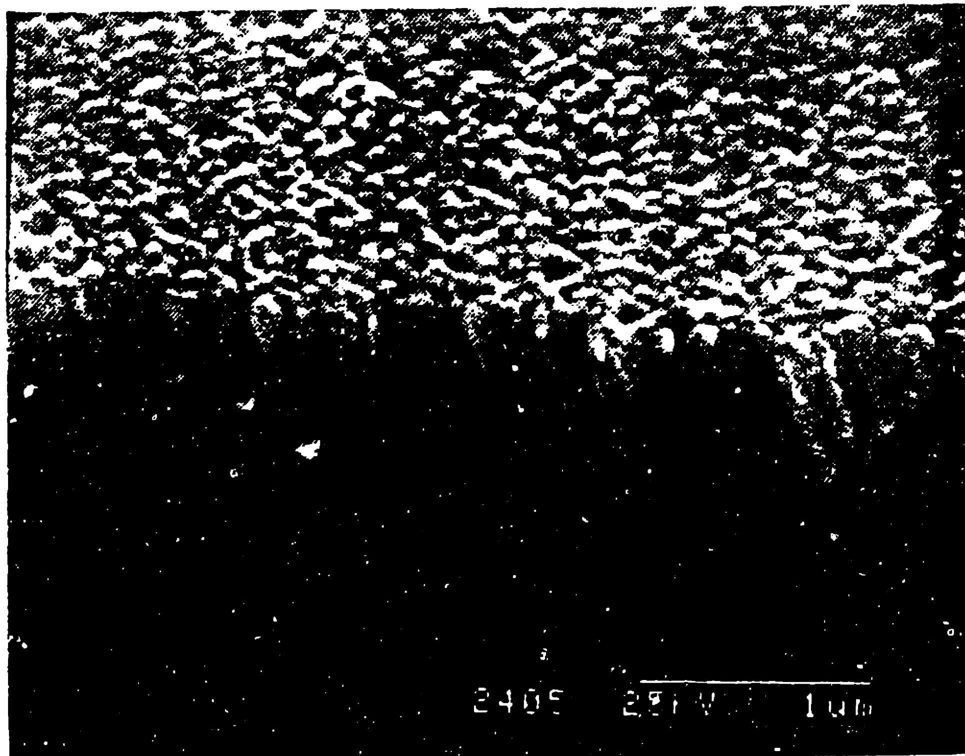

CHAPTER FIVE
DISCUSSION

5.1 Growth Model for Biaxial Alignment from IAD

The columnar structure of the films produced in this study is readily apparent by microstructural examination. The structure near the substrate interface is difficult to characterize, but only those grains which are biaxially aligned grow to dominate the thickness of the film. Crystallites having the (200) orientation perpendicular to the plane of the film grow the fastest even without IAD. These grains ultimately shadow and extinguish the growth of crystallites having orientations other than (200).

Growth of preferred orientations and the extinction of others due to shadowing is well documented for columnar structures [51]. This growth model can be extended to explain the development of biaxial alignment during IAD. Alignment will develop if the net growth rate of columnar grains varies with orientation with respect to the ion beam. Columnar grains of a specific orientation will begin to shadow grains which are growing more slowly. This surface roughness induces a growth instability such that the faster growing grains will begin to dominate the microstructure just as in the case of fiber texture development during film growth. Variation of the columnar growth rate with ion beam orientation can be understood if the etching rate changes with orientation. Ion beam etch rates of single crystals do exhibit minima in the channeling direction of the crystal, as discussed above. A schematic summarizing the key points of the model is shown in Figure 44. Note that this model is based on a growth rate phenomena rather than selective nucleation of specific orientations as proposed by Hasan *et al.* [30]. This alternative view, discussed previously, suggests that misoriented clusters are depleted by ion induced dissociation and sputtering. Those clusters reduced to a subcritical size spontaneously dissociate and either desorb from the surface or contribute to the coarsening of larger, oriented clusters.

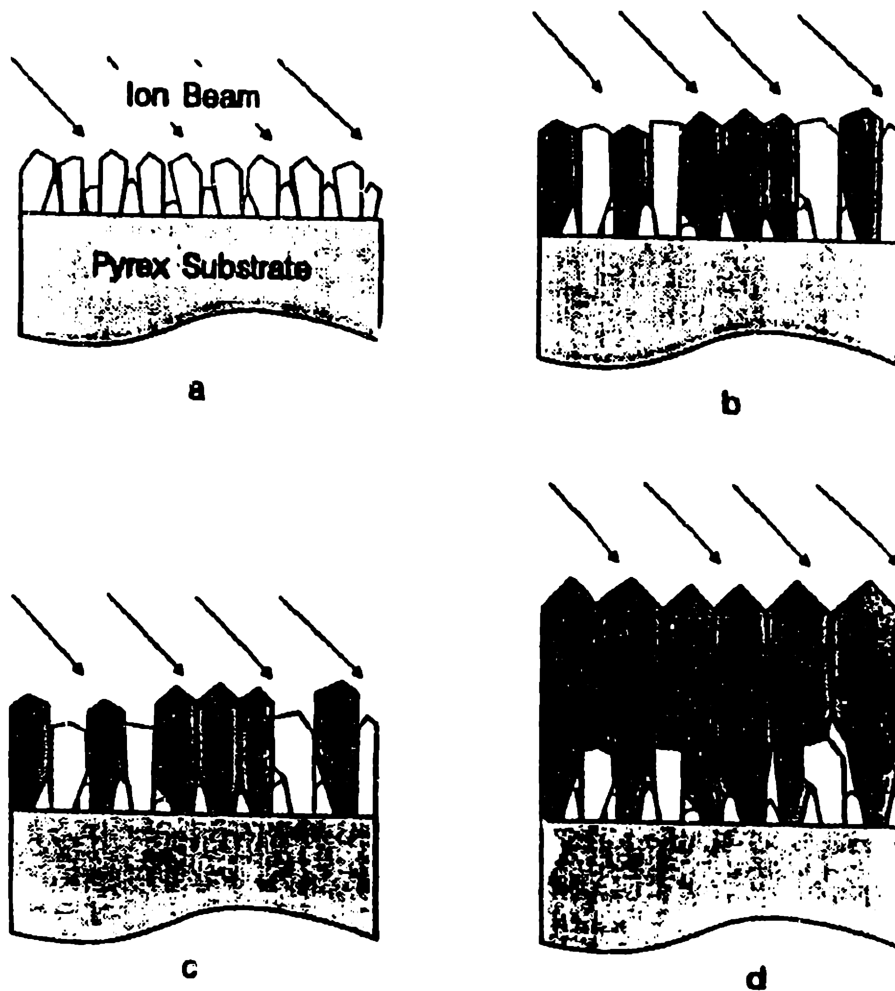

Figure 44. (200) biaxial alignment by IAD due to shadowing of misoriented grains. (a) Initial film deposited is polycrystalline; (b) (200) is the fastest growth direction, so these grains ultimately shadow and extinguish the growth of crystallites having orientations other than (200); (c) alignment develops when the net growth of columnar grains varies with respect to the orientation of the ion beam. Columnar grains of a specific orientation will begin to shadow grains which are growing more slowly; (d) this surface roughness induces a growth instability such that the faster growing, biaxially aligned grains begin to dominate the microstructure.

Evidence for a growth-based selection process can be derived from the experiment where ion beam etching and deposition are carried out at separate times. An already deposited film could be induced to grow with a biaxially aligned structure by etching its surface, as shown in Figure 32. Apparently, low energy ions etch back the pre-deposited and misoriented grains in the film leaving crystallites having preferred orientation extending above the surface. These grains shadow other grains upon subsequent deposition. The experiment demonstrated that in-plane alignment does not occur upon nucleation, but instead is a growth phenomenon. The columnar structure required for this mechanism to occur must develop in films of less than several hundred Angstroms since biaxial alignment develops even though the ion beam is shut off after this thickness. Selective etching of nuclei may occur under some conditions but can not be the only mechanism since an already deposited film can be induced to grow with a biaxially aligned structure.

Observations show that the orientation of the films is a complex function of etching and deposition conditions. Several trends in the selection of some orientations seem to be consistent with the model above. First, beam incidence angles that are close to channeling directions of the (100) columnar grains seem to be preferred. That is, the (220) direction is oriented toward the ion beam when the incidence angle is near 45° and the (111) is oriented toward the beam when the incidence angle is near 35°. The effect is most pronounced at high r values, but the (111) orientation can even be detected at r = 0.05 when $\theta = 38°$. Second, simultaneous etching of the growing film helps to preselect columnar grains with a specific normal orientation. This effect is shown in Figure 26 where the best normal orientation occurs when the ion incidence angle is near 45°.

Evidence for only (220) and (111) orientations with respect to the beam suggests that all other orientations have higher etch rates and are successfully eliminated by the

shadowing process during the growth of the columns. The preponderance of (220) orientation at low *r* values, however, is difficult to explain. The columnar grains are often observed to be at an angle with respect to the substrate, as shown in Figure 31. We have, as yet, noted no systematic trend in this type of structure which correlates with deposition or etching conditions. Sputtering induced surface topography, however, is known to be a complicated function of target microstructure and etching conditions [52]. It seems that this relationship will become even more dependent on experimental conditions during simultaneous deposition. The crystallographic faces of a grain have anisotropic growth rates even without ion bombardment, but in the presence of an ion beam the anisotropy is compounded as the net balance between the growth rate and the etch rate of each face is dependent on the orientation of the grain with respect to the ion beam.

5.2 Comparison with Related Work

IAD experiments by Martin *et al.* [32] demonstrated that an ion beam can be used to induce orientation in ZrO_2 film deposited on glass substrates. The microstructural study they performed in which the ion beam was on only half the time during deposition, resulted in the growth of dense film when the ion beam was on and a porous, columnar structure when the beam was off. From the results Martin *et al.* proposed that the ion induced microstructural changes were a growth phenonemenon and occurred independent of deposition surface. Th ir growth based model agrees with the model for ion induced orientation developed above. Differences in microstructure observed in films deposited on Pyrex and plate glass under identical conditions suggest that the deposition surface is important though the deposition surface did not appear to affect orientation in experiments by Martin *et al.*

Trends in the results of Al-Robaee *et al.* [35,36] and Netterfield *et al.* [37] for the growth of ceria on glass substrates using normal incidence IAD agree with results of

experiments performed here. Their films, like films prepared here, are grown at beam energies of less than 600 eV, have the columnar microstructure and are not fully dense. Netterfield *et al.* [37] attributed the growth of the columnar microstructure suggesting that at 50 - 100 eV, ions do not impart the energy required to increase adatom surface mobility enough to overcome the effects of atomic self-shadowing. The model developed here also cites the effects of atomic self-shadowing as important to the growth of columnar films using low energy IAD. The growth model proposed by Muller 38,39] drew from experimental results by Martin *et al.* [32] and Netterfield *at al.* [37], but emphasized the importance of collision cascades over atomic self-shadowing for the densification of columnar microstructures. Muller mentioned sputtering, a mechanism important to the model developed here, as one effect of ion bombardment, but did not investigate off-normal incidence ion bombardment to include the effects of ion channeling and directional sputtering yield on microstructural development.

Though Yu *et al.* [44,45,46] deposited Nb films and not dielectrics on fused silica substrates, they did produce restricted biaxial alignment in their films with off-normal incidence IAD using a 200 eV Ar^+ beam at an angle 20° from glancing. Bradley *et al.* [47] developed a theory for the orientation of thin films during deposition by off-normal incidence ion bombardment citing the results of Yu *et al.* Bradley *et al.* proposed that ion induced sputtering would be the lowest for orientations in the channeling direction. A net deposition of crystallites oriented in the channeling direction would be possible, therefore, by carefully balancing the ion induced sputtering with the deposition rate. The theory proposed by Bradley *et al.* does not conflict with the model developed here, but their description is simplistic in that it does not duely acknowledge the effects of growth rate anisotropy, sputter yield anisotropy, or atomic self-shadowing on microstructural development.

CHAPTER SIX
CONCLUSIONS

YSZ films deposited without IAD on pyrex substrates are largely amorphous at 200 °C, while those deposited at 600 °C are crystalline and exhibit strong preferred orientation with the (100) axis perpendicular to the plane of the film. Pole figure data from these films confirms the presence of a strong wire texture.

Films produced with IAD exhibit predominantly (200) orientations with respect to the plane of the film, but the (200) reflection intensity varies with bombardment angle and rises to a maximum near 48°. Perfect (100) texture was not observed in any films deposited; (111), (311) and (400) orientations were observed depending on the deposition conditions used.

Different in-plane orientations were observed from the pole figures: biaxially aligned (220), biaxially aligned (111), a mixture of (220) and (111), and uniaxial alignment with (111) wire texture in the direction of the ion beam. Films deposited with ion to atom ratios of 0.05 were (220) biaxially aligned with the quantity of wire texture increasing with beam energy. Those films produced at higher values of *r* were (111) aligned at lower bombardment angles of 8° and 23°, exhibited mixed (111) and (220) orientations at 38°, and showed (220) orientation at 48°.

SEM micrographs reveal that IAD films are columnar in structure and may contain some residual porosity. Film density appears to depend on the angle of ion bombardment, but is affected by other IAD parameters as well. Plan view and cross-sectional TEM and electron diffraction studies indicate that several orientations nucleate on the substrate, but that IAD appears to cause the crystallites having preferred orientation to grow at a relative rate that is larger than those which are misoriented.

A mechanism for the development and growth of biaxially aligned YSZ films on pyrex glass, under the IAD conditions investigated, has been proposed:

The initial film layers deposited are polycrystalline but as the film starts to grow the fast growing (200) oriented grains start to dominate the structure. YSZ films deposited even without IAD on pyrex substrates at 600° C were observed to be crystalline and exhibited strong preferred orientation with the (100) axis perpendicular to the plane of the film. Pole figure data from these films confirm the presence of a strong wire texture. Electron diffraction studies of cross sections biaxially aligned films reveal a polycrystalline region at the interface between the film and the substrate.

The deposition mechanism of these biaxially aligned films is growth controlled, and not nucleation controlled, since films grown separating the film growth from the ion etching stage still show biaxial alignment. Growth rate differentiation creates a microstructural instability caused by shadowing of slower growing grains. The microstructure becomes dominated by those grains which have preferred orientation upon continued growth of the films.

CHAPTER SEVEN
FUTURE WORK

Polycrystalline metal substrates on which a layer of glass has been deposited may be used as an alternative to glass substrates for the base of HTSC multichip modules (MCM). The glass film on the metal would still retain a low dielectric constant to reduce electrical losses. The metal substrate would serve as the ground plane of the device, whereas a ground plane must be added to a glass substrate for it to be used in a MCM. BYC film cracks when deposited on Pyrex or fused quartz substrates due to thermal mismatch. The CTE of Pyrex is 3.25×10^{-6} cm/cm/°C, and the CTE of fused quartz is 0.55×10^{-6} cm/cm/°C, but the CTE of BYC is much larger at 12×10^{-6} cm/cm/°C [53]. Ni has a CTE of 13×10^{-6} cm/cm/°C similar to that of BYC. A thin glass film deposited on top of the Ni substrate assumes a CTE similar to the metal, so cracking would be prevented in the BYC film. To prepare silica films on Ni substrates from a spin-on glass source, the decomposition parameters of the glass must be optimized, and the surface of the resulting glass film should be characterized before a CeO_2 film is deposited using IAD.

Biaxial alignment has been demonstrated on pyrex and soda lime glass substrates, but similar experiments could not be reproduced on quartz and Ni substrates. Different orientations have been reproducibly observed for YSZ and CeO_2 films that were simultaneously deposited on Ni, pyrex, and quartz glass substrates despite careful control of all IAD parameters including deposition rate, bombardment angle, ion current density, and substrate temperature. Analysis of the nature of the substrate morphology, reactivity, and temperature is needed to quantify the effects of surface parameters on the growth of biaxially aligned dielectric films using IAD.

SEM examination of polished, bare glass substrates heated to deposition temperature revealed that well aligned YSZ films were deposited on rough pyrex surfaces, while poorly aligned YSZ films were deposited on smooth quartz surfaces. The surface roughness, therefore, may play an important role in film texture. A more complete evaluation of substrate surface roughness and morphology should be done using atomic force microscopy (AFM) as well as SEM. A study should be conducted in which amorphous and polycrystalline substrates would be polished, ground, and etched by both chemical and ion techniques. The resulting orientation of the CeO_2 films subsequently prepared by IAD could be examined as a function of surface roughness using pole figure analysis and SEM.

While the substrate mounting block was accurately maintained at a constant temperature, various substrate surface temperatures could have resulted due to the different thermal conductivity of each substrate type. The precise substrate surface temperature is difficult to measure, however, especially with clear substrates at low temperatures.

The model illustrated in Figure 44 discusses the development of biaxially aligned microstructure during the growth of ceria and YSZ films on amorphous substrates using IAD, but the model does not address the effects of IAD on initial film growth. The influence of IAD on nucleation and growth could be characterized by depositing films that are on the order of 100 Å thick both with and without IAD. The cluster size, microstructure, and orientation could be studied using SEM, TEM, and electron diffraction. Such experiments would show whether an interfacial layer of continuous film is deposited before the columnar structure begins to form or if the columnar structure develops directly from islands of film deposited on the bare substrate. The influence of substrate surface roughness and chemistry on film growth could be analyzed by depositing thin films on different types of glass substrates including Pyrex, soda lime

glass, fused quartz, and Ni. Ni substrates that have been annealed also should be included to determine the effects of the native oxide layer. Comparison of the microstructure, chemistry, and orientation of films grown on these substrates would show if the film tends to nucleate at defect sites on the substrate surface and if chemical reactions occur between the film and the substrate. The interfacial chemistry of somewhat thicker films could be investigated using Auger electron spectroscopy and X-ray photoelectron spectroscopy (XPS).

REFERENCES

[1] D.K. Fork, S.M. Garrison, M. Hawley, and T.H. Geballe, *J. Mater. Res.* **7**, 1641 (1992).

[2] D.K. Fork, K. Char, F. Bridges, S. Tahara, B.Lairson, J.B. Boyce, G.A.N. Connell, and T.H. Geballe, *Physica C* **162-164**, 121 (1989).

[3] Q. Li, O. Meyer, X.X. Xi, J. Geerk, and G. Linker, *Appl. Phys. Lett.* **55**, 1792 (1989).

[4] L.A. Tietz, C.B. Carter, D.K. Lathrop, S.E. Russek, R.A. Buhrman, and J.R. Michael, *J. Mater. Res.* **4**, 1072 (1989).

[5] W. Shi, J. Shi, J. Sun, W. Yao, and Zh. Qi, *Appl. Phys. Lett.* 57, 822 (1990).

[6] J.P. Zheng, S.Y. Dong, and H.S. Kwok, *Appl. Phys. Lett.* **58**, 540 (1991).

[7] S.M. Garrison, M. Newman, B.F. Cole, K. Char, R.W. Barton, *Appl. Phys. Lett.* **58**, 2168 (1991).

[8] D.K. Fork, D.B. Fenner, R.W. Barton, Julia M. Phillips, G.A.N. Connell, J.B. Boyce, and T.H. Geballe, *Appl. Phys. Lett.* **57**, 1161 (1990).

[9] H. Myoren, Y. Nishiyama, N. Miyamoto, Y. Kai, T. Tamanaka, Y. Osaka, and F. Nishiyama, *Jpn. J. Appl. Phys.* **29**, L955 (1990).

[10] X.D. Wu, R.E. Muenchausen, N.S. Nogar, A. Pique, R. Edwards, B. wilkins, T.S. Ravi, D.M. Huang, and C.Y. Chen, *Appl. Phys. Lett.* **58**, 304 (1991).

[11] K. Char, M.S. Colclough, L.P. Lee, and G. Zaharchuk, *Appl. Phys. Lett.* **59**, 2177 (1991).

[12] Y. Iijima, N. Tanabe, and O. Khono (4th International Symposium on Superconductivity, Oct. 14-17, 1991).

[13] Y. Iijima, N. Tanabe, O. Khono, and Y. Ikeno, *Appl. Phys. Lett.* **60**, 769 (1992).

[14] R.P. Reade, P. Berdahl, R.E. Russo, S.M. Garrison, *Appl. Phys. Lett.* **61**, 2231 (1992).

[15] M.J. Cima, J.S. Schneider, S.C. Peterson, W. Coblenz, *Appl. Phys. Lett.* **53**, 710 (1988).

[16] P.C. McIntyre, MIT; private communication.

[17] B.A. Movchan, and A.V. Demchisin, *Phys. Met. Metallogr.* **28**, 83 (1969).

[18] J.A. Thornton, *Ann. Rev. Mater. Sci.* **7**, 293 (1977).

[19] F.A. Smidt, *Inter. Mater. Rev.* 35, 61 (1990).

[20] C.R.M. Grovenor, H.T.G. Hentzell, and D.A. Smith, *Acta Metall.* **32**, 77 (1984).

[21] R. Messier, *J. Vac. Sci. Tech.* **A4**, 490 (1986).

[22] T. Takgi, *Thin Solid Films* **92**, 1 (1982).

[23] J.E. Greene, and S.A. Barnett, *J. Vac. Sci. Tech.* **21**, 285 (1982).

[24] J.M.E. Harper, J.J. Cuomo, J.R. Gambino, H.R. Kaufman, pp 127-162 in *Ion Bombardment Modification of Surfaces*. Ed. by O. Auciello and R. Kelly. Elsevier, N.Y., 1984.

[25] P.J. Martin, *J. Mater. Sci.* **21**, 1 (1986).

[26] J.J. Cuomo and S.M. Rossnagel, *Nucl. Instr. Meth. in Phys. Res.* **B 19-20**, 963 (1987).

[27] J.E. Greene, "Physics and Chemistry of Film Growth from the Vapor Phase", NATO Advanced Study Institute, Germany, September 1992.

[28] E. Krikorian and R.J. Sneed, *Astrophys. Space Sci.* **65**, 129 (1979).

[29] M. Marinov, *Thin Solid Films* **46**, 267 (1977).

[30] M.-A. Hasan, S.A. Barnett, J.-E. Sundgre, and J.E. Greene, *J.Vac. Sci. Tech.* **A5**, 1883 (1987).

[31] M.-A. Hasan, J. Knall, S.A. Barnett, A. Rockett, J.-E. Sundgre, and J.E. Greene, *J. Vac. Sci. Tech.* **B5**, 1332 (1987).

[32] P.J. Martin, R.P. Netterfield, and W.G. Sainty, *J. Appl. Phys.* **55**, 235 (1984).

[33] P.J. Martin, R.P. Netterfield, W.G. Sainty, W.A. Lanford, and S.H. Sie, *Appl. Phys. Lett.* **43**, 711 (1983).

[34] G. Hass and J.B. Ramsey, *J. Opt. Soc. Am.* **45**, 408A (1955).

[35] M.S. Al-Robaee, K. Narasimha Rao, and S. Mohan, *J. Appl. Phys.* **7**, 2380 (1992).

[36] M.S. Al-Robaee, M. Ghanashyam Krishna, K. Narasimha Rao, and S. Mohan, *J. Vac. Sci. Tech.* **A9**, 3048 (1991).

[37] R.P. Netterfield, W.G. Sainty, P.J. Martin, and S.H. Sie, *Appl. Opt.* **24**, 2267 (1985).

[38] K.-H. Muller, *J. Appl. Phys.* **59**, 2803 (1986).

[39] P.J. Martin and R.P. Netterfield, pp 373-414 in *Handbook of Ion Beam Processing Technology: Principles, Deposition, Film Modification, and Synthesis*. Ed. by J.J. Cuomo, S.M. Rossnagel, and H.R. Kaufman. Noyce Publ., Park Ridge, N.J., 1989.

[40] D. Dobrev, *Thin Solid Films* **92**, 41 (1982).

[41] G.N. Van Wyk and H.J. Smith, *Nucl. Instr. Meth.* **170**, 433 (1980).

[42] G.N. Van Wyk, *Rad. Eff. Lett.* **57**, 45 (1980).

[43] R.M. Bradley, pp 300-314 in *Handbook of Ion Beam Processing Technology: Principles, Deposition, Film Modification, and Synthesis.* Ed. by J.J. Cuomo, S.M. Rossnagel, and H.R. Kaufman. Noyce Publ., Park Ridge, N.J., 1989.

[44] L.S. Yu, J.M.E. Harper, J.J. Cuomo, and D.A. Smith, *Appl. Phys. Lett.* **47**, 932 (1985).

[45] L.S. Yu, J.M.E. Harper, J.J. Cuomo, and D.A. Smith, *J.Vac. Sci. Tech.* **A4**, 443 (1986).

[46] J.M.E. Harper, D.A. Smith, L.S. Yu, and J.J. Cuomo, *Mat. Res. Soc. Symp. Proc.* **51**, 343 (1985).

[47] R.M. Bradley, J.M.E. Harper, and D.A. Smith, *J. Appl. Phys.* **60**, 4160 (1986).

[48] S. Aoki, T. Yamaguchi, Y. Iijima, O. Kohno, S. Nagaya, T. Inoue, (ASC-92, August 24, 1992).

[49] A. Westerheim, Dept. of Mat. Sci. and Engr., MIT, Ph.D. dissertation, 1992.

[50] *Phase Diagrams for Ceramists* **4**, p.141. ED. by R.S. Roth, T. Negas, L.P. Cook. ACS, Columbus, OH, 1981.

[51] A.G. Dirks and H.J. Leamy, *Thin Solid Films* **47**, 219 (1977).

[52] G. Carter, B. Navinsek, J.L. Whitton, p.231 in *Sputtering by Particle Bombardment II, Topics in Applied Pysics* **52**. Ed. by R. Behrisch, Springer-Verlag, Berlin, 1983.

[53] E.A. Geiss, R.L. Sandstrom, W.J. Gallagher, A. Gupta, S.L. Shinde, R.F. Cook, E.I. Cooper, E.J.M. O'Sullivan, J.M. Roldan, A.P. Segmuller, and J. Angilello, *IBM J. of Res. and Dev.* **34**, 6 (1990).